8-2020

Trisections of Flat Surface Bundles over Surfaces

Marla Williams
University of Nebraska - Lincoln, marla.williams@huskers.unl.edu

TRISECTIONS OF FLAT SURFACE BUNDLES OVER SURFACES

by

Marla Williams

A DISSERTATION

Presented to the Faculty of

The Graduate College at the University of Nebraska

In Partial Fulfillment of Requirements

For the Degree of Doctor of Philosophy

Major: Mathematics

Under the Supervision of Professors Alex Zupan and Mark Brittenham

Lincoln, Nebraska

August, 2020

TRISECTIONS OF FLAT SURFACE BUNDLES OVER SURFACES

Marla Williams, Ph.D.

University of Nebraska, 2020

Advisor: Alex Zupan and Mark Brittenham

A trisection of a smooth 4-manifold is a decomposition into three simple pieces with nice intersection properties. Work by Gay and Kirby shows that every smooth, connected, orientable 4-manifold can be trisected. Natural problems in trisection theory are to exhibit trisections of certain classes of 4-manifolds and to determine the minimal trisection genus of a particular 4-manifold.

Let Σ_g denote the closed, connected, orientable surface of genus g. In this thesis, we show that the direct product $\Sigma_g \times \Sigma_h$ has a $((2g+1)(2h+1)+1; 2g+2h)$-trisection, and that these parameters are minimal. We provide a description of the trisection, and an algorithm to generate a corresponding trisection diagram given the values of g and h. We then extend this construction to arbitrary closed, flat surface bundles over surfaces with orientable fiber and orientable or non-orientable base. If the fundamental group of such a bundle has rank $2 - \chi + 2h$, where h is the genus of the fiber and χ is the Euler characteristic of the base, these trisections are again minimal.

ACKNOWLEDGMENTS

I would like to thank my advisors, Alex Zupan and Mark Brittenham, for their patience and support throughout the past four years. You both have taught me so much, and I could not have finished this without you.

To Katie Tucker: thank you for putting up with me as a roommate for five years, for adventuring together, and for always being my friend. Grad school would have looked so much different without you, and I'm glad we went through it together.

To David: you are incredible, and I would not have gotten through this year without you. I am so grateful that we get to move on from grad school together, and I am looking forward to new adventures with you in Virginia.

To the rest of my friends and support system at UNL: you all are amazing, and you brought so much light into my life in Lincoln. I will miss the game nights, the mentor-mentee lunches, the study dates at CoHo, the hours chatting in Avery, and so much more.

Finally, I would like to thank all the trisectors out there who taught me about trisection theory, listened to my ideas, and encouraged me to keep going. I have found so many friends and mentors in this community.

Table of Contents

CHAPTER 1

INTRODUCTION

Four-dimensional topology is the study of *4-manifolds*, topological spaces that are locally homeomorphic to $\mathbb{R}^4$. Since we exist in a 3-dimensional reality, finding accessible ways to visualize, describe, or work with these abstract 4-dimensional spaces can be a challenge. This challenge is compounded by the fact that every finitely-presented group is the fundamental group of some smooth, closed, oriented 4-manifold (see [GS99, Chapter 1]), and even those 4-manifolds with trivial fundamental group are not well-behaved. For example, four is the only dimension in which a smooth n-dimensional manifold may be homeomorphic to $\mathbb{R}^n$ without being diffeomorphic to $\mathbb{R}^n$ (see [GS99, Chapter 1]). A big question, then, is how 4-manifolds might best be studied.

One avenue of approach that was recently introduced by Gay and Kirby [GK16] is the theory of *trisections*, in which a closed, orientable, connected, smooth 4-manifold is broken down into three pieces and all of the 4-dimensional data is encoded on a 2-dimensional surface (see Section 2.4). The allure of trisection theory is that it invokes 2- and 3-dimensional techniques based in *Heegaard theory* to study smooth 4-manifolds; the ubiquity of the trisection structure among smooth 4-manifolds, as illustrated by the following theorem, gives the field its power. Although this theorem is stated for closed 4-manifolds, it extends to *relative trisections* of compact 4-manifolds,

wherein additional structure is imposed to account for the boundary of the 4-manifold [GK16, CGPC18, CIMT19].

Theorem 1.1. *[GK16] Every closed, orientable, connected, smooth 4-manifold admits a trisection, and any two trisections of the same 4-manifold are stably equivalent.*

While the existence of trisections is certainly a useful fact, in practice it is of greater use to know how to trisect a given 4-manifold and how to present a trisection in an accessible way. A *trisection diagram* consists of the closed orientable surface that sits at the core of a trisection, together with three systems of simple closed curves in that surface. Each curve system describes how to attach a set of disks to a thickened copy of the surface in order to reconstruct a 3-dimensional handlebody bounded by the surface. The union of the three resulting handlebodies is called the *spine* of the trisection, and there is a unique way to cap off a thickened spine with 4-dimensional 1-handlebodies to produce a closed, orientable 4-manifold [LP72]. Thus, a trisected 4-manifold can be completely described by a 2-dimensional trisection diagram.

As in the 3-dimensional context of *Heegaard splittings*, the *genus* of a trisection is the genus of the central surface, and the *trisection genus* of a 4-manifold X is the minimum genus of any trisection of X. 4-manifolds with trisection genus g have been classified for $0 \leq g \leq 2$ [GK16, MZ17], and conjecturally classified for $g = 3$ [Mei18]. Additionally, there are larger classes of 4-manifolds that have been explicitly trisected, including 3-manifold bundles over S^1 [Koe17], and 4-manifolds obtained by spinning or twist-spinning a 3-manifold [Mei18]. Both of these constructions use an appropriate choice of *Heegaard diagram* for the associated 3-manifold to obtain a trisection diagram of the 4-manifold. In the relative case for manifolds with boundary, disk bundles over S^2 have been trisected and an algorithm for producing a relative trisection diagram is known [CGPC18] (see Section 5.3).

In Chapter 3, we add trivial *surface bundles over surfaces* to the list of closed 4-manifolds for which trisections and their diagrams are known. The results presented here mirror the Heegaard theoretic results that every Σ_g-bundle over S^1 admits a canonical Heegaard splitting of genus $2g+1$ (see [BR07]) and that these splittings are minimal for trivial bundles [Sch93], as well as for some nontrivial bundles (see Section 2.3):

Theorem 3.3. *For $g \geq 0$, let Σ_g denote the closed, connected, orientable surface of genus g. Then the 4-manifold $X = \Sigma_g \times \Sigma_h$ admits a $((2g+1)(2h+1)+1; 2g+2h)$-balanced trisection.*

Diagrams for these trisections are discussed in Section 3.2 with an algorithm that describes how to construct the trisection surface and the three curve systems. In Section 3.3, we characterize the trisection genus of trivial surface bundles over surfaces using an argument about $\pi_1(\Sigma_g \times \Sigma_h)$:

Theorem 3.17. *The trisection genus of $\Sigma_g \times \Sigma_h$ is $(2g+1)(2h+1)+1$.*

Trivial surface bundles over surfaces are a special case of *flat* surface bundles over surfaces (see Section 2.2). In Chapter 4, we generalize our results for trivial surface bundles to flat surface bundles with orientable fiber. In order for these generalizations to be independent of the orientability of the base surface, the parameters pertaining to the base are now phrased in terms of Euler characteristic rather than genus:

Theorem 4.3. *Let X be a closed, connected, orientable, smooth 4-manifold that fibers as a flat Σ_h-bundle over S, where Σ_h is a closed, connected, orientable surface of genus h and S is a closed, connected surface with Euler characteristic χ. Then X admits a $((3-\chi)(2h+1)+1; 2-\chi+2h)$-balanced trisection.*

For certain flat bundles, these trisections are again minimal:

Proposition 4.6. *Let X be as in Theorem 4.3. If $\pi_1(X)$ has rank $2-\chi+2h$, then the trisection genus of X is $(3-\chi)(2h+1)+1$.*

In Chapter 2, we give the relevant background needed for the proofs in Chapters 3 and 4. Chapter 3 has proofs of Theorems 3.3 and 3.17, and an algorithm that produces a minimal trisection diagram for the direct product of a given pair of surfaces. Chapter 4 gives proofs of Theorem 4.3 and Proposition 4.6, along with an algorithm to create a trisection diagram for a special case of a flat surface bundle over a surface, given the bundle structure. In Chapter 5, we highlight some conjectures and open questions based on these results. Finally, in Appendix A we present some new trisection diagrams resulting from the algorithms in Sections 3.2 and 4.2.

CHAPTER 2

BACKGROUND

This thesis assumes some foundational knowledge of low-dimensional topology, but some of the basic facts we will use are covered in this chapter. See [Hat02, GS99] as references. We begin with an overview of manifolds in Section 2.1, and narrow our focus to fiber bundles in Section 2.2. We then introduce some relevant results from 3-manifold topology in Section 2.3 to lead into a discussion of trisection theory in Section 2.4.

2.1 Compact manifolds

A *(topological) n-manifold* is a Hausdorff, second-countable, topological space M such that every point in M has a neighborhood homeomorphic to an open subset of $\mathbb{R}^n_+ = \{(x_1, \ldots, x_n) \in \mathbb{R}^n \mid x_n \geq 0\}$. The *boundary*, ∂M, of M is the subset of M consisting of all points which do not have a neighborhood homeomorphic to $\mathbb{R}^n$. When M is compact with empty boundary, we say M is a closed manifold. A *chart* is an open subset U of M and a homeomorphism $\varphi : U \to \varphi(U) \subseteq \mathbb{R}^n_+$; an *atlas* on M is a collection of charts that covers M. Given two overlapping charts (U, φ) and (V, ψ), the *transition function* $\varphi \circ \psi^{-1} : \psi(U \cap V) \to \varphi(U \cap V)$ describes how the local Euclidean structures on U and V relate. A *piecewise-linear (PL)* atlas is an atlas for which every

transition function is piecewise-linear; a *smooth* atlas is an atlas for which every transition function is smooth. Recall that smooth means infinitely differentiable. We say an n-manifold M is a PL manifold if a PL atlas for M exists; likewise, M is a smooth manifold if there exists a smooth atlas for M. The 4-manifolds of interest in this thesis are all smooth, which begs the question of distinctions between smooth, PL, and topological manifolds. In general, every smooth manifold is a PL manifold, so the question becomes: when does a manifold have a PL structure, and when is a PL manifold smoothable? For $0 \leq n \leq 3$, there is no distinction between these three categories: every topological n-manifold for $0 \leq n \leq 3$ has a smoothable PL structure that is unique up to isomorphism. For $4 \leq n \leq 7$, every PL manifold is smoothable, but there are n-manifolds with no PL structure, and hence no smooth structure. For $n \geq 8$, there are topological n-manifolds with no PL structure and PL n-manifolds with no smooth structure (see [GS99, Chapter 1], [Mil11]).

Remark 2.1. Unless otherwise specified, manifolds are assumed to be smooth, compact, and orientable throughout this thesis.

A *properly embedded submanifold* N of a manifold M is a subset of M that is itself a manifold with respect to the subspace topology, and that satisfies $\partial N \subseteq \partial M$. We say two submanifolds N_i, $i = 0, 1$ are *smoothly isotopic* if there is a smooth map $f : N \times I \to M$ with $f|_{N\times\{t\}}$ an embedding for all $t \in I$ and $f(N \times \{i\}) = N_i$; two submanifolds with a common boundary are *smoothly isotopic rel boundary* if those smooth maps fix the boundary pointwise. Equivalence of manifolds is considered up to isotopy or diffeomorphism.

The nature of manifolds as spaces that are locally Euclidean makes them prime candidates for study. Some key questions that arise involve classification—what manifolds exist?—and methodology—what tools exist to study manifolds, particularly

when those manifolds can not be immersed or embedded in 3-space? It is a well-known fact that the circle, S^1, is the only closed, connected 1-manifold. Furthermore, any compact 1-manifold that is connected but not closed is homeomorphic to I, the unit interval in $\mathbb{R}$. Manifolds of dimension 2 are commonly called *surfaces*, and while there is more nuance in the form a 2-manifold can take, the classification of surfaces is still a well-known result. Any orientable, closed, connected surface is homeomorphic to an n-fold connect sum of tori, $\Sigma_n = \#^n T^2$, for some $n \geq 0$, where $\Sigma_0 = \#^0 T^2$ is taken to be the 2-sphere, S^2. Any non-orientable, closed, connected surface is homeomorphic to a k-fold connect sum of real projective planes, $F_k = \#^k \mathbb{RP}^2$, for some $k \geq 1$. Replacing "closed" with "compact" expands this collection of surfaces to include $\Sigma_{n,b}$ and $F_{k,b}$, which denote the compact, connected surfaces obtained by iteratively removing the interior of a disk from (the interior of) $\Sigma_{n,b-1}$ or $F_{k,b-1}$, respectively, where $\Sigma_{n,0} = \Sigma_n$ and $F_{k,0} = F_k$. Here, the numbers n and k count the genus of the surface and b counts the number of boundary components, each of which is homeomorphic to S^1.

Remark 2.2. Throughout this thesis, we use Σ_n, $\Sigma_{n,b}$, and F_k to denote compact, connected surfaces as described above.

Manifolds of dimension higher than two are more challenging to describe or classify. One approach for smooth manifolds involves handles and handle decompositions (see [GS99, Chapter 4] for more detail, including a discussion of framing). Given integers $n \geq k \geq 0$, an *n-dimensional k-handle* is a copy of $B^k \times B^{n-k}$ attached to the boundary of an n-manifold M along $\partial B^k \times B^{n-k} \cong S^{k-1} \times B^{n-k}$ by a smooth embedding $\rho : \partial B^k \times \partial B^{n-k} \to \partial M$. To stay in the realm of orientable manifolds, we require ρ to be orientation-preserving. The subset $B^k \times \{0\}$ is called the *core* of the handle, and its boundary $S^{k-1} \times \{0\}$ is the *attaching sphere*; the subset $\{0\} \times B^{n-k}$

is called the *co-core*, and its boundary $\{0\} \times S^{n-k-1}$ is the *belt sphere*. In the case where $n = 3$, the different types of handles are shown in Figure 2.1 with the cores, co-cores, and attaching regions indicated.

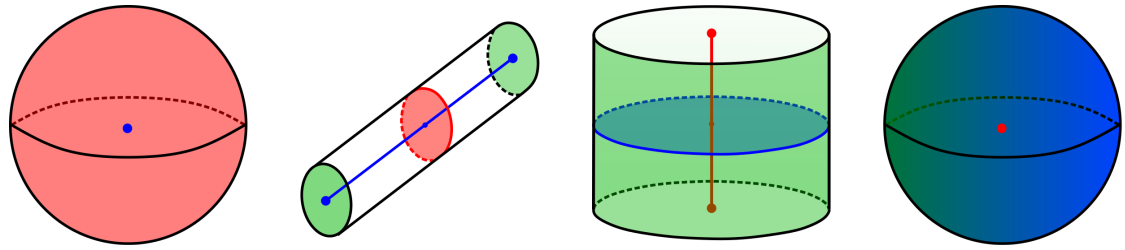

$B^0 \times B^3$
core: $B^0 \times \{0\}$
co-core: $\{0\} \times B^3$
att. region: $\emptyset$

$B^1 \times B^2$
core: $B^1 \times \{0\}$
co-core: $\{0\} \times B^2$
att. reg.: $S^0 \times B^2$

$B^2 \times B^1$
core: $B^2 \times \{0\}$
co-core: $\{0\} \times B^2$
att. reg.: $S^1 \times B^1$

$B^3 \times B^0$
core: $B^3 \times \{0\}$
co-core: $\{0\} \times B^0$
att. reg.: $S^2 \times B^0$

Figure 2.1: From left to right, a 3-dimensional 0-handle, 1-handle, 2-handle, and 3-handle

When the attaching sphere of a k-handle meets the belt sphere of a $(k-1)$-handle transversely at a single point, we say the handles form a cancelling pair: attaching these two handles amounts to taking a boundary connect sum with B^n, which does not change the diffeomorphism-type of the manifold. Another type of handle move is a *handle slide*, in which one k-handle is slid over another, where $0 < k < n$. Formally, consider two k-handles h_1 and h_2 attached to ∂M. A handle slide of h_1 over h_2 is described by an isotopy that takes the attaching sphere A of h_1 in $\partial(M \cup h_2)$ and pushes it through the belt sphere B of h_2.

A *handle decomposition* of a smooth n-manifold M is a way of breaking down M into handles. In particular, if M is compact, we express ∂M as a disjoint union $\partial_+ M \sqcup \partial_- M$ of compact submanifolds, and identify M with a manifold obtained from $I \times \partial_- M$ by attaching handles, so that $\partial_- M$ corresponds naturally to $\{0\} \times \partial_- M$.

Note that any handle decomposition has a *dual* decomposition, which may be thought of as "flipping" the original decomposition and replacing each k-handle with an $(n-k)$-handle (see [GS99, Chapter 4]). Since attaching maps are defined up to isotopy, we may assume that the handles in a handle decomposition are attached in increasing order of *index*, where the index of a k-handle is defined to be k. Under this assumption, a theorem of Cerf states that any two handle decompositions for a compact pair $(M, \partial_- M)$ are related by a sequence of handle slides, isotopies, and the introduction or deletion of cancelling handle pairs [Cer70]. If M is connected and compact but not closed, then ∂M is not empty, and we may assume that a handle decomposition of M has no 0-handles (if $\partial_- M \neq \emptyset$) or no n-handles (if $\partial_+ M \neq \emptyset$). Conversely, if M is connected and closed, then $\partial M = \emptyset$, so the first handle attachment is necessarily a 0-handle, and the last handle attachment is necessarily an n-handle. Moreover, we may assume there is exactly one 0-handle in this case, as the connectedness of M would have 1-handles cancelling any extra 0-handles; the dual decomposition correspondingly grants that we may assume there is exactly one n-handle when M is connected and closed. Whenever $\partial_- M$ is empty, we call M with a given handle decomposition a handlebody.

Much of our work in this thesis concerns 3- and 4-dimensional handlebodies consisting of a single 0-handle and some number of 1-handles, as described further in Sections 2.3 and 2.4. However, we do make use of more general handle decompositions, and Section 3.3 relies on the relationship between a handle decomposition of a manifold X and a presentation of $\pi_1(X)$. Specifically, given a manifold X with one 0-handle, each 1-handle determines a generator of $\pi_1(X)$, with relations given by the attaching circle of each 2-handle.

2.2 Fiber bundles

Because manifolds get more complicated as the dimension increases, a reasonable question is how one might construct a new manifold from a manifold or manifolds of smaller dimension. The method most relevant to this thesis is a fiber bundle, which is locally a direct product of two manifolds.

Definition 2.3. A *fiber bundle* E has the form $F \to E \xrightarrow{p} B$, where p is a continuous map from the *total space*, E, to the *base* space, B, and for each $x \in B$, the set $p^{-1}(\{x\})$ is homeomorphic to the *fiber*, F. Additionally, for each $x \in B$, there is a neighborhood V_x of x and a homeomorphism $q_x : V_x \times F \to p^{-1}(V_x)$ such that $(p \circ q_x)(x', y) = x'$ for all $(x', y) \in V_x \times F$. We say E is an F-bundle over B.

A *section* of a bundle $F \to E \xrightarrow{p} B$ is a continuous map $f : B \to E$ satisfying $p(f(x)) = x$ for each $x \in B$. Given a subset A of B and a section f of an F-bundle over B, we say $f(A)$ is a *section over* A. We call an F-bundle over B *trivial* when it is homeomorphic to the direct product $B \times F$ and p is projection onto the first coordinate; otherwise, a nontrivial bundle structure carries some global twisting. Every fiber bundle is locally trivial: if U_1 and U_2 are two open sets in B such that $p^{-1}(U_i) \cong U_i \times F$, then there is a map $U_1 \cap U_2 \to \mathrm{Diff}(F)$ that determines how these local trivializations are glued to obtain $p^{-1}(U_1 \cup U_2)$. Applying this to an appropriate open cover of B produces the full bundle structure, thus the diffeomorphism group $\mathrm{Diff}(F)$ of F is called the *structure group* of an F-bundle over B. Low-dimensional examples of trivial bundles include the annulus $A = S^1 \times I = I \times S^1$, and the torus $T^2 = S^1 \times S^1$. Low-dimensional examples of nontrivial bundles include the Möbius band, which is a twisted I-bundle over S^1, and the Klein bottle, which is a twisted S^1-bundle over S^1. These examples are shown in Figure 2.2 with the factor manifolds marked in red and blue. It is worth noting that the roles of fiber and base may always

be swapped in trivial bundles, but it is not necessary for a nontrivial F-bundle over B to also have the structure of a nontrivial B-bundle over F. Additionally, although the nontrivial bundles shown in Figure 2.2 are non-orientable, orientable nontrivial bundles exist and are prevalent in other dimensions.

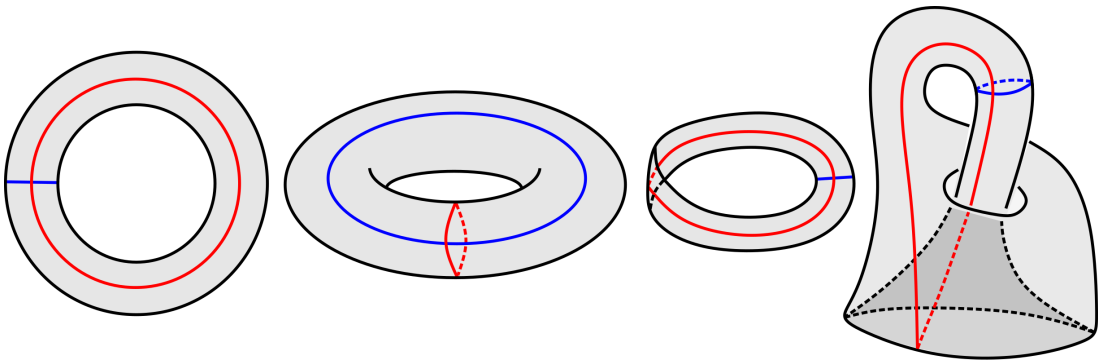

Figure 2.2: Examples of 2-dimensional fiber bundles

The class of fiber bundles in which the fiber is a surface are called *surface bundles*, and these have a special representation known as the *monodromy representation*, which measures how the fiber transforms over a loop γ in the base (see [ST20]). In particular, for any n-manifold B, a Σ_g-bundle over B determines a homomorphism $\varphi : \pi_1(B) \to \mathrm{MCG}(\Sigma_g)$, where $\mathrm{MCG}(\Sigma_g)$ is the *mapping class group* of Σ_g. That is, $\mathrm{MCG}(\Sigma_g) = \mathrm{Diff}(\Sigma_g)/\mathrm{Diff}_0(\Sigma_g)$ is the quotient of the diffeomorphism group of Σ_g by diffeomorphisms isotopic to the identity, which gives the group of isotopy classes of (orientation-preserving) diffeomorphisms of Σ_g; this group is finitely generated by *Dehn twists* about curves in Σ_g (see [FM12, Chapter 4]). The homomorphism φ is called the monodromy representation of the Σ_g-bundle, and when $g \geq 2$, this representation uniquely determines the bundle [EE67]. A surface bundle is called *flat* if the induced monodromy representation lifts to a map $\tilde{\varphi} : \pi_1(B) \to \mathrm{Diff}(\Sigma_g)$; conjecturally, every surface bundle is flat (see [MT19]). In this case, a homotopy class of loops in the base space corresponds to a particular diffeomorphism of the fiber,

rather than just an isotopy class of diffeomorphisms. We will use this in Section 4.2 to describe flat bundles more explicitly, as part of our constructions.

2.3 3-manifolds and Heegaard splittings

In this section, we take a closer look at 3-manifolds through the lens of Heegaard theory. [Sch01] is a good resource for a more complete picture. By convention, we refer to a 3-dimensional handlebody with a single 0-handle, g 1-handles, and no 2- or 3-handles as a genus g 3-dimensional handlebody, or simply a genus g handlebody when the dimension is clear from context. However, it will sometimes be useful to use the dual handle decomposition to think of a genus g handlebody H as the result of attaching g 2-handles and one 3-handle to $\{1\} \times \partial H \subseteq I \times \partial H$, where $\partial H \cong \Sigma_g$.

A *genus g Heegaard splitting* of a closed, connected 3-manifold M is a decomposition $M = H_1 \cup_\Sigma H_2$, where H_1 and H_2 are genus g handlebodies with a common boundary: the *Heegaard surface* $\Sigma \cong \Sigma_g$. In essence, this is just a handle decomposition of M, where H_1 is the union of the 0- and 1-handles of M, H_2 is the union of the 2- and 3-handles of M, and Σ is the surface between them. As mentioned previously, we can reconstruct H_i from $I \times \Sigma$ by attaching g 2-handles to $\{1\} \times \Sigma$ and then capping off the resulting spherical boundary component with a 3-handle. If we embed the attaching circles of the 2-handles for H_1 and H_2 into Σ to obtain a system of $2g$ curves on the Heegaard surface, we may denote the curves corresponding to H_1 by $\boldsymbol{\alpha} = (\alpha_1, \ldots, \alpha_g)$, and the curves corresponding to H_2 by $\boldsymbol{\beta} = (\beta_1, \ldots, \beta_g)$. Then $(\Sigma; \boldsymbol{\alpha}, \boldsymbol{\beta})$ is called a *Heegaard diagram* for this splitting of M, and it is uniquely determined up to handle slides within each curve set, isotopy of the curves within Σ, and homeomorphism of Σ. Any genus g Heegaard splitting of a 3-manifold M may be *stabilized* to a genus $g+1$ splitting by adding a cancelling pair of 1- and 2-handles to

the handle decomposition defining the splitting. The effect on the diagram, beyond increasing the genus of Σ by one, is to add a pair of curves α_{g+1} and β_{g+1} that meet transversely at a single point and are disjoint from the pre-existing curves. Conversely, if such a pair of curves exist, they correspond to a cancelling pair of handles, and the splitting may be *destabilized* (thus, reducing the genus by one) by eliminating the handle pair. The corresponding destabilization within the diagram may be seen as compressing Σ along one of these curves and omitting the other. We will not go into much detail here, but there is a generalization of Heegaard splittings to compact 3-manifolds, wherein the two pieces of the splitting are *compression bodies*, or relative handlebodies, which may have nonempty negative boundary (in the sense of the handle decompositions discussed in Section 2.1). In this case, the Heegaard surface Σ is homeomorphic to $\partial_+ H_i$ for $i = 1, 2$, and $\partial M = \partial_- H_1 \cup \partial_- H_2$.

A classic result of 3-manifold topology is that every compact, connected, orientable 3-manifold admits a Heegaard splitting. Additionally, the Reidemeister-Singer Theorem states that any two splittings of the same 3-manifold have a common stabilization [Rei33, Sin33]. Thus, we have a reasonable 3-manifold invariant in the form of the *Heegaard genus*, which is the minimum genus of a Heegaard splitting for a given 3-manifold M.

The utility of these existence and uniqueness results is enhanced by abundant examples of Heegaard diagrams and constructions for splitting different types of 3-manifolds. One method in particular that motivates the techniques used in Chapter 4 involves splitting surface bundles over the circle. Recognizing a Σ_g-bundle over S^1 as the mapping torus of a function $f : \Sigma_g \to \Sigma_g$, the monodromy representation of the bundle takes the generator of $\pi_1(S^1)$ to $[f] \in \mathrm{MCG}(\Sigma_g)$. The canonical splitting of such a bundle has genus $2g + 1$, where the splitting surface is two copies of the fiber joined by two tubes, the first of which connects the two fibers, while the second

bumps the genus up by one. The S^1 factor of the bundle roughly corresponds to a loop in the Heegaard surface that starts in one copy of the fiber, crosses to the other copy along one of the added tubes, and crosses back along the other tube. Following that path around, the monodromy is applied and this affects the curve system that describes the 2-handles for one of the handlebodies. Minimality of this construction is addressed in part in [ST93, Rub05], as there are examples of Σ_g-bundles over S^1 with Heegaard genus 2, for arbitrarily large g. However, in some cases these genus $2g+1$ splittings of $\Sigma_g \to M \xrightarrow{p} S^1$ are minimal. In particular, if $M \cong S^1 \times \Sigma_g$ is a trivial bundle, or if the monodromy of $\Sigma_g \to M \xrightarrow{p} S^1$ is a sufficiently large power of a pseudo-Anosov map, then the Heegaard genus of M is $2g+1$ (see [Sch93, Rub05], and Section 5.1).

2.4 4-manifolds and trisections

4-manifolds fall into a sort of limbo between low-dimensional and high-dimensional topology: many techniques and theorems that apply to n-manifolds for $n \geq 5$ or $n \leq 3$ fail in dimension 4. For instance, for smooth n-manifolds X and Y, we say Y is an *exotic* X if Y is homeomorphic but not diffeomorphic to X. For $n \neq 4$, there is no notion of an exotic $\mathbb{R}^n$; however, exotic $\mathbb{R}^4$'s exist [Gom83]. Even within this dimension, where any finitely presented group is the fundamental group of some smooth 4-manifold, the class of smooth simply-connected 4-manifolds is vast and not well-understood. Various approaches to the study of 4-manifolds exist, but we will focus on *trisection theory*, which is a natural 4-dimensional analogue of Heegaard theory. Throughout this section and this thesis, we refer to 4-dimensional handlebodies that consist of a single 0-handle and g 1-handles (but no 2-, 3-, or 4-handles) as *4-dimensional 1-handlebodies of genus g*; note that these handlebodies are diffeomorphic

to $\natural^g(S^1 \times B^3)$.

In 2012, Gay and Kirby introduced trisections of smooth 4-manifolds as an analogue of Heegaard splittings of 3-manifolds, and proved the following:

Theorem 1.1. *[GK16] Every closed, orientable, connected, smooth 4-manifold admits a trisection, and any two trisections of the same 4-manifold are stably equivalent.*

Unlike a Heegaard splitting that splits the manifold into two 3-dimensional handlebodies with a common boundary, a trisection decomposes a 4-manifold into three 4-dimensional 1-handlebodies; these handlebodies intersect only on their (3-dimensional) boundaries, and the common intersection of all three together is a closed, orientable surface. Similar to a Heegaard diagram for a 3-manifold, a trisection diagram is a collection of curves in this surface, now with three systems of g curves when the surface has genus g. In particular, each pair of curve systems is a Heegaard diagram for a connect sum of $S^1 \times S^2$'s. As in the 3-dimensional case, these curves are attaching circles for 3-dimensional 2-handles, giving us the spine of the trisection, which is the union of the boundaries of the 4-dimensional 1-handlebodies. By a theorem of Laudenbach and Poénaru [LP72], there is a unique way to cap off this spine with 4-dimensional 1-handlebodies to obtain a closed 4-manifold, and hence, a trisection diagram uniquely determines a closed 4-manifold up to diffeomorphism. Figure 2.3 shows a trisection diagram of the 4-torus, which is the Cartesian product of four circles; this diagram was generated using the algorithm in Section 3.2. We proceed with a formal definition, and some existing results.

Definition 2.4. [GK16] Let X be a closed, connected, orientable, smooth 4-manifold. A $(g; k_1, k_2, k_3)$-*trisection* of X is a quadruple $(\Sigma; X_1, X_2, X_3)$ satisfying the following conditions:

- $X = X_1 \cup X_2 \cup X_3$;

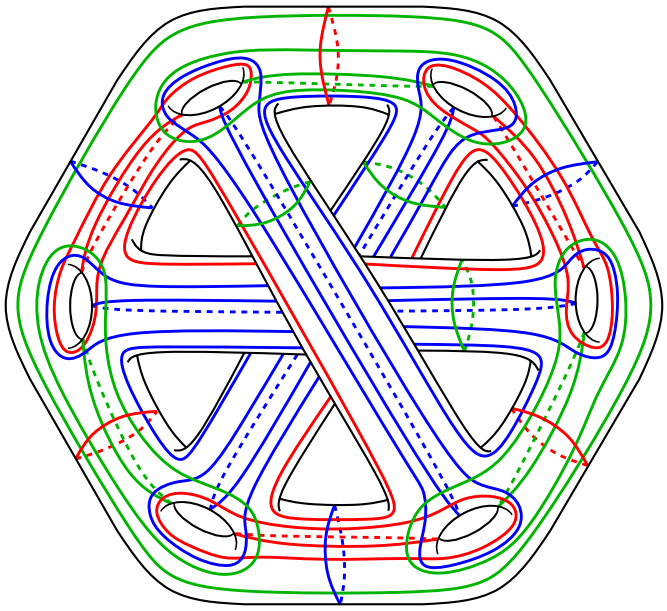

Figure 2.3: A trisection diagram for $T^4 = T^2 \times T^2$

- X_i is a 4-dimensional 1-handlebody of genus k_i for $i \in \{1, 2, 3\}$;
- $X_i \cap X_j$ is a 3-dimensional handlebody of genus g for $i \neq j$; and
- $\Sigma = X_1 \cap X_2 \cap X_3$ is a closed, orientable surface of genus g.

The *genus* of the trisection is the genus g of Σ. If $k_1 = k_2 = k_3$, we call the trisection *balanced* and refer to it as a $(g; k_1)$-trisection of X; otherwise, it is *unbalanced*.

As with Heegaard splittings of 3-manifolds, there is a notion of trisection stabilization that corresponds to taking a connect sum of a trisected manifold X with S^4. For $\{i, j, \ell\} = \{1, 2, 3\}$, this adds the neighborhood of a properly embedded, boundary parallel arc in $X_j \cap X_\ell$ to X_i and removes that neighborhood from each of X_j and X_ℓ; the new trisection surface is taken to be the triple intersection of the new 4-dimensional 1-handlebodies. Stabilization will not change k_j or k_ℓ, but will increase g and k_i each by one, where again, X_i is the sector to which we added the neighborhood of an arc. Theorem 1.1 states that any two trisections of the same

4-manifold have a common stabilization [GK16]. Analogous to the Heegaard genus of a 3-manifold, we say the *trisection genus* of a 4-manifold X is the minimum genus over all trisections of X. Additionally, Gay and Kirby define a relative trisection of a compact 4-manifold, in which context some results about existence and uniqueness up to stabilization have again been shown [CGPC18, CIMT19].

Existing constructions of trisections and their diagrams are limited, but actively growing. We remind the reader that 4-manifolds with trisection genus g have been completely classified for $0 \leq g \leq 2$ [GK16,MZ17], and conjecturally classified for $g = 3$ [Mei18]. Additionally, 3-manifold bundles over S^1 have been trisected in [Koe17], while 4-manifolds obtained by spinning and twist-spinning 3-manifolds have been trisected in [Mei18]; these last two constructions each use a Heegaard diagram for the associated 3-manifold to build a trisection diagram of the 4-manifold. In this thesis, we trisect flat surface bundles over surfaces and present an algorithm to generate a corresponding trisection diagram when both the base and the fiber are orientable and the flat structure satisfies an additional hypothesis regarding fixed points. The techniques used in trisecting these bundles are inspired by the canonical Heegaard splitting of a Σ_g-bundle over S^1 discussed in Section 2.3, and by the relative trisections of disk bundles over S^2 presented in [CGPC18].

CHAPTER 3

TRISECTING TRIVIAL SURFACE BUNDLES OVER SURFACES

In this chapter, we trisect direct products of closed, orientable surfaces. In particular, fix $g, h \geq 0$ and let $X^4 = \Sigma_g \times \Sigma_h$ be the trivial Σ_h-bundle over Σ_g. Section 3.1 describes a decomposition of X into $X = X_1 \cup X_2 \cup X_3$, and presents a proof that this structure is a $((2g+1)(2h+1)+1; 2g+2h)$-trisection of X. In Section 3.2, we state and prove an algorithm for producing a trisection diagram corresponding to this trisection of X. Finally, we prove in Section 3.3 that this trisection is minimal and the trisection genus of X is $(2g+1)(2h+1)+1$.

3.1 A trisection of $X^4 = \Sigma_g \times \Sigma_h$

Before describing the trisection of X, we first produce a particular decomposition of our base surface, Σ_g, that we will use throughout this chapter.

Lemma 3.1. *Σ_g admits a cell structure consisting of $4g+2$ vertices, $6g+3$ edges, and three faces. In particular, we write $\Sigma_g = B_1 \cup B_2 \cup B_3$, subject to the following:*

- *Each B_i is diffeomorphic to a closed 2-disk B^2.*

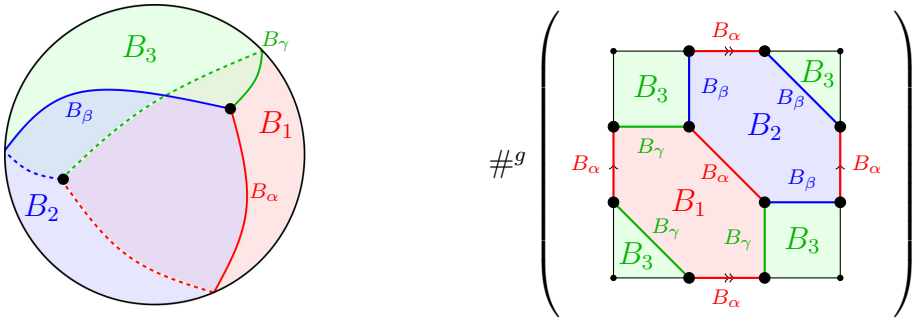

(a) A disk decomposition of $\Sigma_0 = S^2$ (b) A disk decomposition of $\Sigma_g = \#^g T^2$.

Figure 3.1: Disk decompositions of base surfaces

- *The pairwise intersections of these disks are* $B_\alpha = B_1 \cap B_2$, $B_\beta = B_2 \cap B_3$, *and* $B_\gamma = B_3 \cap B_1$; *each is a pairwise disjoint collection of* $2g+1$ *edges and may be enumerated as* $B_\alpha = \sqcup_{i=1}^{2g+1} B_\alpha^i$, *etc.*

- *The triple intersection* $B_1 \cap B_2 \cap B_3 = \partial B_\alpha = \partial B_\beta = \partial B_\gamma$ *is a disjoint union of* $4g+2$ *vertices. We refer to this set as* V.

Proof. The decomposition shown in Figure 3.1 suffices, with the connect sum taken at an appropriate pair of vertices, as shown in Figure 3.2 for Σ_2; iterating produces a decomposition for Σ_g. □

Remark 3.2. In the constructions that follow, we will always use the decomposition demonstrated in Figure 3.1.

Let p be the bundle map $\Sigma_h \to X^4 \xrightarrow{p} \Sigma_g$, and let $q_1, q_2, q_3 \in \Sigma_h$ be distinct points in the fiber surface Σ_h, with pairwise disjoint closed neighborhoods $N_i := N(q_i)$ each diffeomorphic to B^2. It is worth noting that each $q_i \notin \partial N_i$. Then for each $i = 1, 2, 3$, we have that $B_i \times \{q_i\} \subseteq p^{-1}(B_i)$ is a section over B_i. Furthermore, these sections are pairwise disjoint and have pairwise disjoint tubular neighborhoods

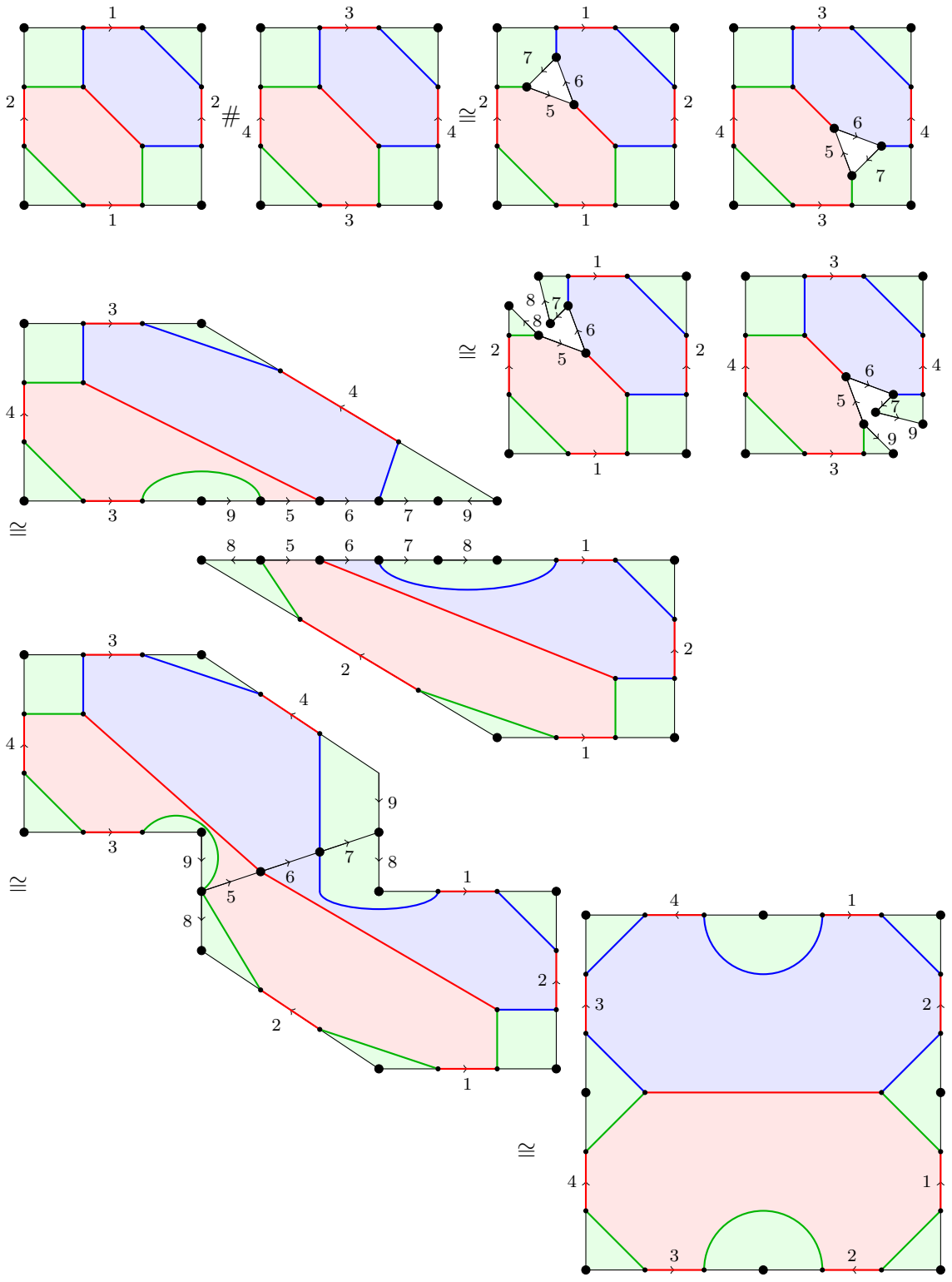

Figure 3.2: Forming a decomposition of a genus 2 surface by taking the connect sum of two tori

$\nu_i := B_i \times N_i \subseteq p^{-1}(B_i)$. With indices taken mod 3, define

$$X_i = \overline{p^{-1}(B_i) \setminus \nu_i} \cup \nu_{i+1} \tag{3.1}$$

for $i = 1, 2, 3$.

Theorem 3.3. *With X_1, X_2, X_3 defined as in (3.1), let $\Sigma := X_1 \cap X_2 \cap X_3$. Then $(\Sigma; X_1, X_2, X_3)$ is a $((2g+1)(2h+1)+1; 2g+2h)$-balanced trisection of $X = \Sigma_g \times \Sigma_h$.*

Remark 3.4. Following Definition 2.4, proving Theorem 3.3 amounts to proving the following four claims:

- $X = X_1 \cup X_2 \cup X_3$.
- For each $i = 1, 2, 3$, we have $X_i \cong \natural^{2g+2h}(S^1 \times B^3)$.
- For each pair $1 \leq i \neq j \leq 3$, the intersection $X_i \cap X_j = \partial X_i \cap \partial X_j$ is diffeomorphic to $\natural^{(2g+1)(2h+1)+1}(S^1 \times B^2)$.
- $\Sigma = \partial(X_i \cap X_j) \cong \Sigma_{(2g+1)(2h+1)+1}$.

The last two points are primarily addressed by Lemmas 3.5 and 3.7; the remainder of the proof of Theorem 3.3 is postponed for now.

Lemma 3.5. *Let X_1, X_2, X_3 be as in (3.1). For each pair $1 \leq i \neq j \leq 3$, the intersection $X_i \cap X_j$ is a 3-dimensional handlebody with genus $(2g+1)(2h+1)+1$. That is, $X_i \cap X_j \cong \natural^{(2g+1)(2h+1)+1}(S^1 \times B^2)$.*

Proof. Let $i = 1$ and $j = 2$; the other cases follow by a change of indices, since for any pair $i \neq j$, one is the successor of the other. Then $X_i \cap X_j = X_1 \cap X_2$ consists of the following four pieces: (a) $\overline{p^{-1}(B_1) \setminus \nu_1} \cap \overline{p^{-1}(B_2) \setminus \nu_2}$, (b) $\nu_2 \cap \overline{p^{-1}(B_2) \setminus \nu_2}$, (c) $\overline{p^{-1}(B_1) \setminus \nu_1} \cap \nu_3$, and (d) $\nu_2 \cap \nu_3$. We will describe each part in turn before

looking at how their intersections determine the attaching maps that yield the union of these four pieces.

(a) The first piece, $\overline{p^{-1}(B_1) \setminus \nu_1} \cap \overline{p^{-1}(B_2) \setminus \nu_2}$, consists of $2g+1$ pairwise disjoint copies of a genus $2h+1$ 3-dimensional handlebody. Indeed, the definitions of p and ν_i give us that

$$\overline{p^{-1}(B_1) \setminus \nu_1} \cap \overline{p^{-1}(B_2) \setminus \nu_2} = \left[B_1 \times \left(\overline{\Sigma_h \setminus N_1}\right)\right] \cap \left[B_2 \times \left(\overline{\Sigma_h \setminus N_2}\right)\right],$$

which is easily recognized as

$$(B_1 \cap B_2) \times \left(\overline{\Sigma_h \setminus (N_1 \sqcup N_2)}\right). \tag{3.2}$$

The first factor here is equal to $\left(\sqcup_{i=1}^{2g+1} B_\alpha^i\right)$ by definition of B_α, while the second factor is a copy of $\Sigma_{h,2}$. Hence, we have

$$\overline{p^{-1}(B_1) \setminus \nu_1} \cap \overline{p^{-1}(B_2) \setminus \nu_2} \cong \sqcup_{2g+1} (I \times \Sigma_{h,2}).$$

Since the thickened compact surface $I \times \Sigma_{h,b}$, for $b \geq 1$, is a genus $2h+b-1$ 3-dimensional handlebody, we thus conclude that this first piece of $X_1 \cap X_2$ is a pairwise disjoint collection of handlebodies, each with genus $2h+1$:

$$\overline{p^{-1}(B_1) \setminus \nu_1} \cap \overline{p^{-1}(B_2) \setminus \nu_2} \cong \sqcup_{2g+1} \natural^{2h+1} (S^1 \times B^2).$$

(b) The second piece, $\nu_2 \cap \overline{p^{-1}(B_2) \setminus \nu_2}$, is a solid torus, depicted in Figure 3.3. The definition of p and ν_2 let us see that

$$\nu_2 \cap \overline{p^{-1}(B_2) \setminus \nu_2} = (B_2 \times N_2) \cap \left(B_2 \times \left(\overline{\Sigma_h \setminus N_2}\right)\right) = B_2 \times \partial N_2. \tag{3.3}$$

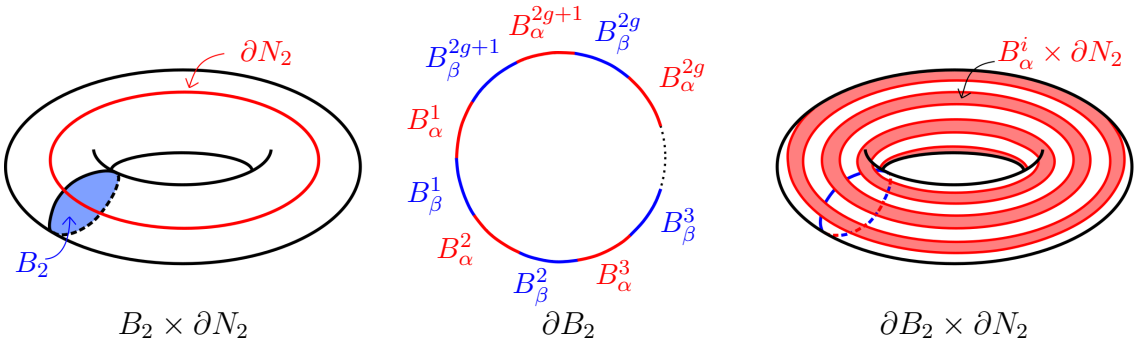

Figure 3.3: On the left, we have the solid torus $B_2 \times \partial N_2$. In the middle, we have the boundary of B_2 expressed as the union of $\sqcup B_\alpha^i$ and $\sqcup B_\beta^j$ (up to reordering). On the right, we see the collection of parallel annuli $\{B_\alpha^i \times \partial N_2\}_{i=1}^{2g+1}$ in $\partial B_2 \times \partial N_2$.

Since both B_2 and N_2 are homeomorphic to a 2-disk, it follows that the direct product $B_2 \times \partial N_2 \cong B^2 \times S^1$ is a solid torus.

Notice that the boundary of this solid torus is the torus $\partial B_2 \times \partial N_2$, which can be decomposed into $4g+2$ parallel annuli using the structure of ∂B_2 (see Figure 3.3). In particular, since $\partial B_2 = (B_1 \cap B_2) \cup (B_2 \cap B_3) = \left(\sqcup_{i=1}^{2g+1} B_\alpha^i\right) \cup \left(\sqcup_{j=1}^{2g+1} B_\beta^j\right)$, we can express this toroidal boundary as

$$\partial B_2 \times \partial N_2 = \left(\sqcup_{i=1}^{2g+1} (B_\alpha^i \times \partial N_2)\right) \cup \left(\sqcup_{i=1}^{2g+1} (B_\beta^i \times \partial N_2)\right). \tag{3.4}$$

(c) The third piece, $\overline{p^{-1}(B_1) \setminus \nu_1} \cap \nu_3$, is a collection of $2g+1$ pairwise disjoint 3-balls, each of which will be considered as a 3-dimensional 1-handle $I \times B^2$: notice that

$$\overline{p^{-1}(B_1) \setminus \nu_1} \cap \nu_3 = \left(B_1 \times \left(\overline{\Sigma_h \setminus N_1}\right)\right) \cap (B_3 \times N_3) = (B_1 \cap B_3) \times N_3,$$

with the first equality coming from the definition of p and ν_i, and the second equality a consequence of N_3 being contained in $\overline{\Sigma_h \setminus N_1}$. Recall from Lemma

3.1 that we defined $B_\gamma = \sqcup_{i=1}^{2g+1} B_\gamma^i$ as the intersection of B_1 with B_3. Hence,

$$\overline{p^{-1}(B_1) \setminus \nu_1} \cap \nu_3 = B_\gamma \times N_3 = \sqcup_{i=1}^{2g+1} (B_\gamma^i \times N_3) \cong \sqcup_{2g+1} B^3 \tag{3.5}$$

is the disjoint union of $2g+1$ 3-balls, each with the inherent structure of $I \times B^2$ in our product 4-manifold.

(d) The final piece, $\nu_2 \cap \nu_3$, is empty by construction, since ν_2 and ν_3 were chosen to be disjoint.

To see how these three nonempty pieces combine to form $X_1 \cap X_2$, we first consider the intersection of the solid torus from (b) with the collection of handlebodies from (a). Since $\left[(B_1 \cap B_2) \times \left(\overline{\Sigma_h \setminus (N_1 \sqcup N_2)}\right)\right] \cap [B_2 \times \partial N_2] = (B_1 \cap B_2) \times \partial N_2$, this intersection is a pairwise disjoint collection of $2g+1$ annuli. Moreover, recall from (3.4) that these annuli are all parallel in $\partial B_2 \times \partial N_2$, the boundary of the solid torus from (b), as shown in Figure 3.3. We now observe that each component annulus $B_\alpha^i \times \partial N_2$ of this collection is essential in the boundary of exactly one of the $2g+1$ handlebodies and disjoint from the rest. Each handlebody is the thickened twice-punctured surface $B_\alpha^i \times \left(\overline{\Sigma_h \setminus (N_1 \sqcup N_2)}\right)$ for some $1 \leq i \leq 2g+1$, and has the genus $2h+1$ surface $S_i = \left[\partial B_\alpha^i \times \left(\overline{\Sigma_h \setminus (N_1 \sqcup N_2)}\right)\right] \cup [B_\alpha^i \times (\partial N_1 \sqcup \partial N_2)]$ as its boundary. Since ∂B_α^i is two discrete points, we have expressed the surface S_i as the union of two copies of $\Sigma_{h,2}$, with the boundary components of one connected to those of the other by the annuli $B_\alpha^i \times \partial N_1$ and $B_\alpha^i \times \partial N_2$. Schematically, this looks like Figure 3.4 (in the case where $h = 3$), with the annulus $B_\alpha^i \times \partial N_2$ highlighted as the intersection of this component handlebody with the solid torus $B_2 \times \partial N_2$.

Consider the union of the handlebodies from (a) and the solid torus from (b) by starting with the solid torus and attaching the handlebodies one by one. We see that

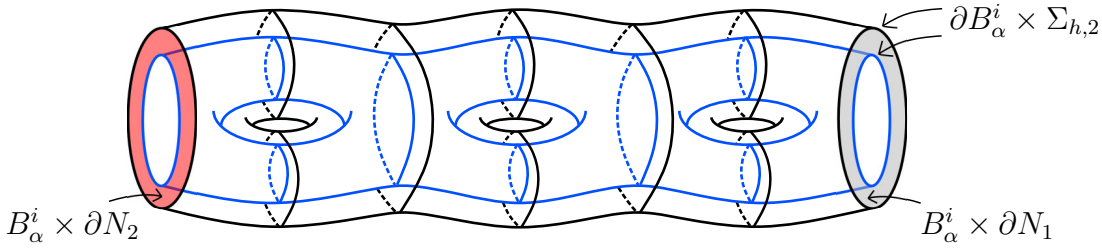

Figure 3.4: One boundary component of $\overline{p^{-1}(B_1) \setminus \nu_1} \cap \overline{p^{-1}(B_2) \setminus \nu_2}$, with the essential annulus $B^i_\alpha \times \partial N_2$ highlighted in red as the intersection with $\nu_2 \cap \overline{p^{-1}(B_2) \setminus \nu_2}$.

each successive attachment of a genus $2h+1$ handlebody along the common annulus depicted in Figure 3.4 will increase the genus (of the component containing the solid torus) by $2h$. Overall, we attach a total of $2g+1$ handlebodies of genus $2h+1$ to the solid torus, which has genus 1. Alternatively, note that each attachment reduces both the total genus and the number of connected components by 1; therefore, when we begin with $2g+2$ connected components and a total genus of $(2g+1)(2h+1)+1$, gluing until we have a single connected component will likewise reduce the total genus by $2g+1$. From either perspective, the result is a genus $(2g+1)(2h)+1$ handlebody.

We now need to attach the $2g+1$ 3-balls from (c). This amounts to attaching $2g+1$ 1-handles to the existing handlebody, as evidenced by the following three observations. First, that by (3.5), the collection of 3-balls can be described as $B_\gamma \times N_3$, which is contained in X_1 and hence is equal to $X_1 \cap (B_\gamma \times N_3)$. Second, that the genus $(2g+1)(2h)+1$ handlebody that was just constructed is $X_1 \cap \overline{p^{-1}(B_2) \setminus \nu_2}$, which can be rewritten as $X_1 \cap \left(B_2 \times \left(\overline{\Sigma_h \setminus N_2}\right)\right)$. Third, that intersecting these yields $\sqcup_{i=1}^{2g+1} \left((\partial B^i_\gamma) \times N_3\right)$, the attaching regions for $2g+1$ 1-handles, as detailed below: from our first observation and the fact that N_3 is contained in $\overline{\Sigma_h \setminus N_2}$, we get

$$\begin{aligned}[B_\gamma \times N_3] \cap \left[X_1 \cap \left(B_2 \times \left(\overline{\Sigma_h \setminus N_2}\right)\right)\right] &= \left[\sqcup_{i=1}^{2g+1} (B^i_\gamma \times N_3)\right] \cap \left[B_2 \times \left(\overline{\Sigma_h \setminus N_2}\right)\right] \\ &= \sqcup_{i=1}^{2g+1} \left(\left(\partial B^i_\gamma\right) \times N_3\right).\end{aligned}$$

Note that for each $1 \leq i \leq 2g+1$, the direct product $\partial B^i_\gamma \times N_3$ is a pair of 2-disks that function as the attaching regions for the 1-handle $B^i_\gamma \times N_3$. Thus, the intersection $X_1 \cap X_2$ is diffeomorphic to $\natural^{(2g+1)(2h+1)+1}(S^1 \times B^2)$. As the X_i are defined symmetrically, it is immediate that $X_1 \cap X_3$ and $X_2 \cap X_3$ also have this form. $\square$

Remark 3.6. The form of the triple intersection $X_1 \cap X_2 \cap X_3$ follows from the conditions that each X_i is a 4-dimensional 1-handlebody and each $X_i \cap X_j$ is a 3-dimensional handlebody. Nonetheless, the proof of Lemma 3.7 gives an explicit description of the surface $\Sigma = X_1 \cap X_2 \cap X_3$, and this description will be useful in Section 3.2.

Lemma 3.7. *Let X_1, X_2, X_3 be as in* (3.1)*, and define $\Sigma := X_1 \cap X_2 \cap X_3$ as their triple intersection. Then $\Sigma \cong \Sigma_{(2g+1)(2h+1)+1}$.*

Notation. Throughout the proofs of both Lemma 3.7 and Theorem 3.3, we use $\Sigma_{h,3}$ to denote the particular surface $\overline{\Sigma_h \setminus (N_1 \sqcup N_2 \sqcup N_3)}$, namely, the genus h fiber surface with three boundary components of the form ∂N_i.

Proof of Lemma 3.7. From (3.2), (3.3), (3.5) in the proof of Lemma 3.5, we have that

$$X_1 \cap X_2 = (B_2 \times \partial N_2) \cup_{B_\alpha \times \partial N_2} \left(B_\alpha \times \left(\overline{\Sigma_h \setminus (N_1 \sqcup N_2)} \right) \right) \cup_{V \times N_3} (B_\gamma \times N_3)\,;$$

permuting indices demonstrates that

$$X_2 \cap X_3 = (B_3 \times \partial N_3) \cup_{B_\beta \times \partial N_3} \left(B_\beta \times \left(\overline{\Sigma_h \setminus (N_2 \sqcup N_3)} \right) \right) \cup_{V \times N_1} (B_\alpha \times N_1)\,.$$

We will consider Σ, the triple intersection of X_1, X_2, X_3 as the intersection of $X_1 \cap X_2$ and $X_2 \cap X_3$ using the above descriptions. To that end, we make several observations:

(i) $\partial N_2 \cap \partial N_3$ is empty by construction, so $(B_2 \times \partial N_2) \cap (B_3 \times \partial N_3) = \emptyset$.

(ii) $B_\gamma \subseteq B_3$ and $\partial N_3 \subseteq N_3$, so $(B_3 \times \partial N_3) \cap (B_\gamma \times N_3) = B_\gamma \times \partial N_3$.

(iii) $B_3 \cap B_\alpha = V$, and ∂N_3 is contained in $\overline{\Sigma_h \setminus (N_1 \sqcup N_2)}$, so their intersection is ∂N_3. Hence, the intersection of $B_3 \times \partial N_3$ with $B_\alpha \times \left(\overline{\Sigma_h \setminus (N_1 \sqcup N_2)}\right)$ is $V \times \partial N_3$, which is contained in $B_\gamma \times \partial N_3$, from (ii).

(iv) $B_\beta \subseteq B_2$ and $\partial N_2 \subseteq \overline{\Sigma_h \setminus (N_2 \sqcup N_3)}$, so $(B_2 \times \partial N_2) \cap \left(B_\beta \times \left(\overline{\Sigma_h \setminus (N_2 \sqcup N_3)}\right)\right)$ is equal to $B_\beta \times \partial N_2$.

(v) $B_\beta \cap B_\gamma = V$ and $N_3 \cap \overline{\Sigma_h \setminus (N_2 \sqcup N_3)} = \partial N_3$, so the intersection of $B_\gamma \times N_3$ with $B_\beta \times \left(\overline{\Sigma_h \setminus (N_2 \sqcup N_3)}\right)$ is $V \times \partial N_3$, again contained in (ii).

(vi) $B_\beta \cap B_\alpha = V$ and $\left(\overline{\Sigma_h \setminus (N_1 \sqcup N_2)}\right) \cap \left(\overline{\Sigma_h \setminus (N_2 \sqcup N_3)}\right) = \Sigma_{h,3}$. Thus, the intersection of $B_\alpha \times \left(\overline{\Sigma_h \setminus (N_1 \sqcup N_2)}\right)$ and $B_\beta \times \left(\overline{\Sigma_h \setminus (N_2 \sqcup N_3)}\right)$ is $V \times \Sigma_{h,3}$.

(vii) $N_1 \cap \partial N_2$ is empty by construction, so $(B_\gamma \times N_3) \cap (B_\alpha \times N_1) = \emptyset$.

(viii) $N_1 \cap N_3$, too, is empty by construction, so $(B_\gamma \times N_3) \cap (B_\alpha \times N_1) = \emptyset$.

(ix) $N_1 \cap \left(\overline{\Sigma_h \setminus (N_1 \sqcup N_2)}\right) = \partial N_1$, so $B_\alpha \times \left(\overline{\Sigma_h \setminus (N_1 \sqcup N_2)}\right)$ and $B_\alpha \times N_1$ intersect along $B_\alpha \times \partial N_1$.

The union of these nine pieces is $(X_1 \cap X_2) \cap (X_2 \cap X_3)$; as three (i, vii, viii) are empty and a fourth (ii) contains two others (iii, v), we are left with four relevant nonempty pieces. In particular: the piece from (vi) is $V \times \Sigma_{h,3}$ and can be recognized as $4g + 2$ copies of $\Sigma_{h,3}$, the fiber with three disks removed; the pieces from (ii), (iv), and (ix) are $B_\gamma \times \partial N_3$, $B_\beta \times \partial N_2$, and $B_\alpha \times \partial N_1$, respectively, each of which is a pairwise disjoint collection of $2g + 1$ annuli.

We now see that there is a natural bijection between the boundary components of $V \times \Sigma_{h,3}$ and the collective boundary components of $B_\gamma \times \partial N_3$, $B_\beta \times \partial N_2$, and

$B_\alpha \times \partial N_1$. Indeed, the former has boundary $\sqcup_{i=1}^{3} \sqcup_{x \in V} (\{x\} \times \partial N_i)$, which is

$$(\sqcup_{x \in V}(\{x\} \times \partial N_3)) \sqcup (\sqcup_{x \in V}(\{x\} \times \partial N_2)) \sqcup (\sqcup_{x \in V}(\{x\} \times \partial N_1)) .$$

But this is easily recognized as $\partial(B_\gamma \times \partial N_3) \sqcup \partial(B_\beta \times \partial N_2) \sqcup \partial(B_\alpha \times \partial N_1)$. As these annuli and copies of $\Sigma_{h,3}$ do not otherwise intersect, it follows that their union amounts to identifying their boundaries. Thus, we have

$$\Sigma = [B_\gamma \times \partial N_3] \cup_{V \times \partial N_3} [(B_\beta \times \partial N_2) \cup_{V \times \partial N_2} (V \times \Sigma_{h,3})] \cup_{V \times \partial N_1} [B_\alpha \times \partial N_1] . \quad (3.6)$$

To see that this surface has genus $(2g+1)(2h+1)+1$, note that the copies of $\Sigma_{h,3}$ contribute a total genus of $(4g+2)(h) = (2g+1)(2h)$, as each component has genus h and there are $|V| = 4g+2$ components. Attaching $B_\beta \times \partial N_2 = \sqcup_{i=1}^{2g+1}(B_\beta^i \times \partial N_2)$ connects these surface components in pairs. This eliminates all boundary components of the form $\{x\} \times \partial N_2$, for $x \in V$, reduces the number of connected components to $2g+1$, and leaves the total genus as $(2g+1)(2h)$, where now each connected component is homeomorphic to $\Sigma_{2h,2}$.

Attaching $B_\gamma \times \partial N_3$ likewise connects the thrice-punctured fibers in pairs; we claim this happens in such a way that the result is a connected surface of genus $(2g+1)(2h)+1$ with $4g+2$ boundary components. This is evident from the initial decomposition of the base surface, Σ_g, into $B_1 \cup B_2 \cup B_3$. Recall that B_3 has boundary $B_\beta \cup B_\gamma$ homeomorphic to S^1. Since each of B_β and B_γ consists of $2g+1$ pairwise disjoint edges, and $B_\beta \cap B_\gamma = V$ is a discrete set of $4g+2$ distinct points, it follows that ∂B_3 has the form shown in Figure 3.1 with edges alternating between B_β and B_γ. Thus, for each $1 \leq i \leq 2g$, attaching the annulus $B_\gamma^i \times \partial N_3$ reduces the number of connected components by one, eliminates two boundary components of the form

$\{x\} \times \partial N_3$, and has no effect on the total genus.

There are now $2g+2$ annuli remaining, along with a copy of $\Sigma_{(2g+1)(2h),4g+4}$, where exactly two of the latter's boundary components have the form $\{x\} \times \partial N_3$. These are eliminated by attaching the final component of $B_\gamma \times \partial N_3$, which increases the total genus by 1. Similarly, attaching each component of $B_\alpha \times \partial N_1$ will eliminate two boundary components of the form $\{x\} \times \partial N_1$, and increase the genus by 1. In the end, the surface is closed and connected, with genus $(2g+1)(2h)+1+(2g+1)$. Thus, we have established our claim that $\Sigma \cong \Sigma_{(2g+1)(2h+1)+1}$. □

We now introduce one more useful lemma, before proceeding with the proof of Theorem 3.3 as outlined in Remark 3.4.

Lemma 3.8. *Let M and N be compact, n-dimensional submanifolds of an n-manifold Y. If $M \cap N$ is a nonempty $(n-1)$-manifold, then $M \cap N = \partial M \cap \partial N$.*

Proof. Suppose M and N are compact, n-dimensional submanifolds of an n-manifold Y, such that $M \cap N$ is a nonempty $(n-1)$-manifold. Furthermore, suppose for the sake of contradiction that for some $x \in M \cap N$, we have $x \notin \partial M$. Then, there is an open neighborhood $U \cong \mathbb{R}^n$ of x in M such that U is also open in Y, so $U \cap N$ contains an n-ball. But $U \cap N$ is contained in $M \cap N$, which contradicts our assumption that this intersection is an $(n-1)$-manifold. Therefore, $x \in \partial M \cap \partial N$. □

Proof of Theorem 3.3. We first show that $X = X_1 \cup X_2 \cup X_3$. This is immediate from the definition of each X_i, since

$$\begin{aligned} X_1 \cup X_2 \cup X_3 &= \left[\overline{p^{-1}(B_1) \setminus \nu_1} \cup \nu_2\right] \cup \left[\overline{p^{-1}(B_2) \setminus \nu_2} \cup \nu_3\right] \cup \left[\overline{p^{-1}(B_3) \setminus \nu_3} \cup \nu_1\right] \\ &= \cup_{i=1}^3 p^{-1}(B_i) = p^{-1}\left(\cup_{i=1}^3 B_i\right) = p^{-1}(\Sigma_g) = X. \end{aligned}$$

Having established that X is the union of the X_i, we will now show that X_i is a 4-dimensional 1-handlebody with genus $2g+2h$, for each $i = 1, 2, 3$. Without loss of generality, let $i = 1$. By definition of p, the preimage of B_1 under p is $p^{-1}(B_1) = B_1 \times \Sigma_h$. Moreover, since $\nu_1 = B_1 \times N_1$ and both B_1 and N_1 are diffeomorphic to B^2, it follows that

$$\overline{p^{-1}(B_1) \setminus \nu_1} = B_1 \times \left(\overline{\Sigma_h \setminus N_1}\right) \cong B^2 \times \Sigma_{h,1} \cong \natural^{2h}(S^1 \times B^3).$$

Thus, this piece of X_1 is a 4-dimensional 1-handlebody with genus $2h$. To this we attach ν_2, a 4-ball, along the $2g+1$ pairwise disjoint 3-balls that comprise the intersection of these sets, as demonstrated below. Since ν_1 and ν_2 are disjoint, we first note that $\nu_2 \cap \left(\overline{p^{-1}(B_1) \setminus \nu_1}\right) = \nu_2 \cap p^{-1}(B_1)$. From the definition of ν_2 and p, we recognize this second expression as $(B_2 \times N_2) \cap (B_1 \times \Sigma_h)$. As N_2 is a disk contained in Σ_h, and $B_1 \cap B_2 = B_\alpha$ is diffeomorphic to a disjoint union of $2g+1$ intervals, it follows that

$$(B_2 \times N_2) \cap (B_1 \times \Sigma_h) = (B_1 \cap B_2) \times N_2 = B_\alpha \times N_2 \cong \sqcup_{i=1}^{2g+1} B^3.$$

Hence, attaching ν_2 to $\overline{p^{-1}(B_1) \setminus \nu_1}$ amounts to adding $2g$ 1-handles to $\natural^{2h}(S^1 \times B^3)$. The result is that $X_1 \cong \natural^{2g+2h}(S^1 \times B^3)$ is a genus $2g+2h$ 4-dimensional 1-handlebody. An identical argument demonstrates the same for X_2 and X_3.

From Lemma 3.5, we know that the pairwise intersections $X_i \cap X_j$ for each $i \neq j$ are each diffeomorphic to $\natural^{(2g+1)(2h+1)+1}(S^1 \times B^2)$. It follows from Lemma 3.8 that X_1 and X_2 intersect only on their boundaries; by symmetry, the same holds for the pair X_1 and X_3, and for the pair X_2 and X_3.

Similarly, Lemma 3.7 established that Σ is a closed, connected, orientable surface

of genus $(2g+1)(2h+1)+1$; a second application of Lemma 3.8 yields the relationship $\Sigma = \partial(X_i \cap X_j)$ for each pair $1 \leq i \neq j \leq 3$. □

3.2 A diagram algorithm for trivial bundles

The simplest interesting example of the algorithm implementation is the trivial T^2-bundle over S^2, that is, the direct product $S^2 \times T^2$, where we have $g = 0$ and $h = 1$. We will first motivate the curve algorithm with this example, then state and prove the algorithm in general, and follow with the mirrored example of $T^2 \times S^2$, where $g = 1$ and $h = 0$. Additionally, we show that the trisection diagrams obtained in Examples 3.9 and 3.15 are equivalent.

As in Section 3.1, we let $\Sigma_{h,3}$ denote the particular surface $\overline{\Sigma_h \setminus (N_1 \sqcup N_2 \sqcup N_3)}$, namely, the genus h fiber surface with three boundary components of the form ∂N_i for some $1 \leq i \leq 3$. The proof of Lemma 3.7 gave a description of the trisection surface Σ as the union of $V \times \Sigma_{h,3}$, $B_\gamma \times \partial N_3$, $B_\beta \times \partial N_2$, and $B_\alpha \times \partial N_1$. Noting that the 1-skeleton of the decomposition $\Sigma_g = B_1 \cup B_2 \cup B_3$ of the base surface is $V \cup B_\gamma \cup B_\beta \cup B_\alpha$, we can thus think of obtaining Σ from this 1-skeleton in the following way. First, replace each vertex with a copy of $\Sigma_{h,3}$. Each edge will then be replaced by a single annular component of $(B_\alpha \times \partial N_1) \sqcup (B_\beta \times \partial N_2) \sqcup (B_\gamma \times \partial N_3)$. A careful labeling of the vertices and edges in the 1-skeleton gives a natural bijection with this collection of punctured fibers and annuli that corresponds to how these pieces are glued to obtain Σ.

Example 3.9. First note that with $g = 0$ and $h = 1$, our trisection surface Σ has genus $(2g+1)(2h+1)+1 = 4$. We begin with a disk decomposition of the base, S^2, and extract the 1-skeleton, as seen in Figure 3.5.

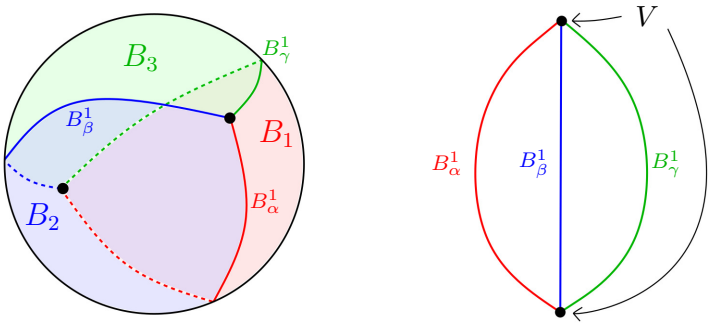

Figure 3.5: At left, the base sphere as the union of three 2-disks; at right, the 1-skeleton of this decomposition.

We then obtain Σ from this graph as shown in Figure 3.6, recognizing our trisection surface as $\Sigma = (V \times \Sigma_{1,3}) \cup (B_\alpha^1 \times \partial N_1) \cup (B_\beta^1 \times \partial N_2) \cup (B_\gamma^1 \times \partial N_3)$.

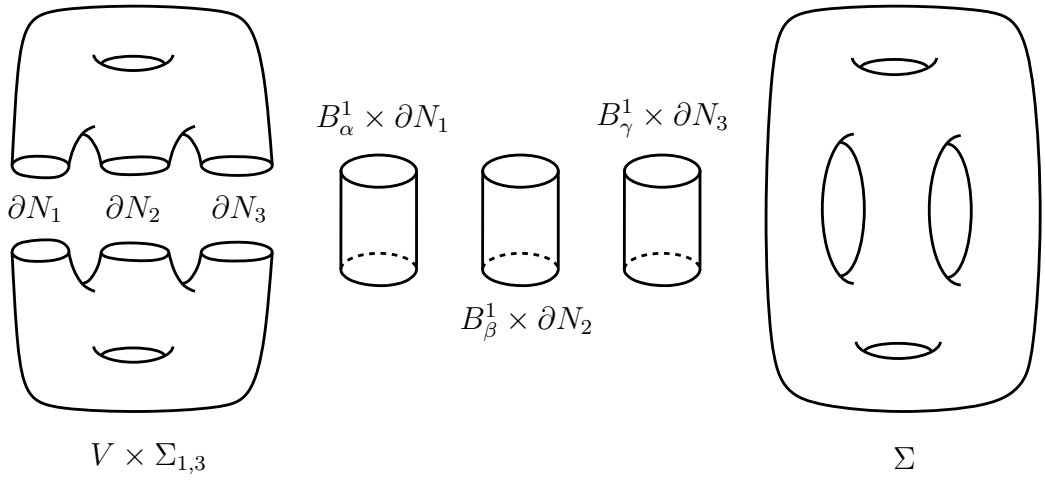

Figure 3.6: Constructing Σ from the 1-skeleton of the base disk decomposition.

To add our first curve system, we let $\boldsymbol{\alpha} = (\alpha_1, \alpha_2, \alpha_3, \alpha_4)$ denote a complete system of curves in Σ that describes the 3-dimensional handlebody $X_1 \cap X_2$, described as follows. We start by choosing arcs ω_α^1 and ω_α^2 in $\Sigma_{1,3}$ such that these arcs are disjoint, simple, properly embedded with endpoints in ∂N_1, and such that

$\overline{\Sigma_{1,3} \setminus (\omega_\alpha^1 \sqcup \omega_\alpha^2)}$ is a pair of pants. Additionally, we let Ω_α denote $\omega_\alpha^1 \sqcup \omega_\alpha^2$, and choose a simple properly embedded arc $\mathcal{C}_\alpha$ in $\overline{\Sigma_{1,3} \setminus \Omega_\alpha}$ that has endpoints c_α^1 in $\partial N_1 \setminus \partial\Omega_\alpha$ and c_α^2 in ∂N_2. Ω_α and $\mathcal{C}_\alpha$ can be seen in Figure 3.7a. Our first curve, α_1, will be $\{b_\gamma^1\} \times \partial N_3$, where b_γ^1 denotes the midpoint of the edge B_γ^1 (see Figure 3.7b). For the curves α_2 and α_3, we set $\alpha_2 = (\partial B_\alpha^1 \times \omega_\alpha^1) \cup (B_\alpha^1 \times \partial\omega_\alpha^1)$ and $\alpha_3 = (\partial B_\alpha^1 \times \omega_\alpha^2) \cup (B_\alpha^1 \times \partial\omega_\alpha^2)$. These curves are shown in Figure 3.7c, and will be described in more detail in the proof of the algorithm later on. To place our final $\boldsymbol{\alpha}$ curve, we define $\alpha_4 = (\partial B_\alpha^1 \times \mathcal{C}_\alpha) \cup (B_\alpha^1 \times \{c_\alpha^1\}) \cup (B_\beta^1 \times \{c_\alpha^2\})$, as shown in Figure 3.7d.

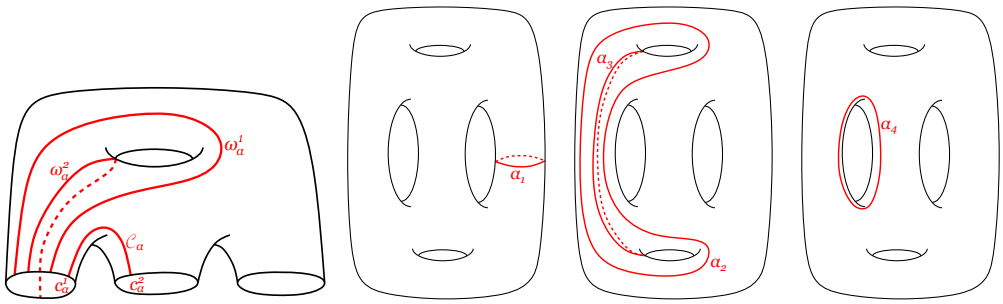

Figure 3.7: Placing the $\boldsymbol{\alpha}$ curves on Σ, a trisection surface for $S^2 \times T^2$.

Our remaining curve sets are obtained in a similar fashion, with $\boldsymbol{\beta}$ describing $X_2 \cap X_3$ and $\boldsymbol{\gamma}$ describing $X_3 \cap X_1$. We end up with the trisection diagram shown in Figure 3.8.

We are now ready to introduce the curve algorithm in full generality, given our trisection surface $\Sigma = (V \times \Sigma_{h,3}) \cup (B_\alpha \times \partial N_1) \cup (B_\beta \times \partial N_2) \cup (B_\gamma \times \partial N_3)$.

Notation. For each $\delta \in \{\alpha, \beta, \gamma\}$ and each $1 \leq i \leq 2g+1$, let b_δ^i denote the midpoint of the edge B_δ^i in Σ_g.

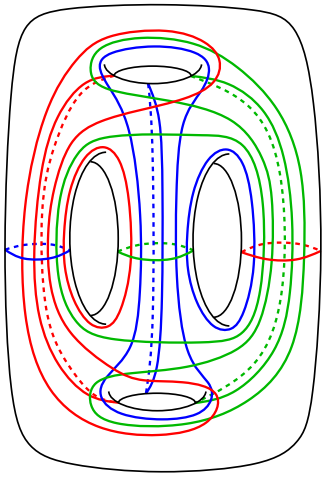

Figure 3.8: A trisection diagram for $S^2 \times T^2$.

Remark 3.10. The final steps of this algorithm involve a permutation of indices. We remind the reader that the permutation $(\alpha\beta\gamma)(123)$ on the set $\{\alpha, \beta, \gamma, 1, 2, 3\}$ is the bijection $\alpha \mapsto \beta \mapsto \gamma \mapsto \alpha$, $1 \mapsto 2 \mapsto 3 \mapsto 1$ that cyclically permutes each of the subsets $\{\alpha, \beta, \gamma\}$ and $\{1, 2, 3\}$. Thus, a second iteration of this permutation is the map $\alpha \mapsto \gamma \mapsto \beta \mapsto \alpha$, $1 \mapsto 3 \mapsto 2 \mapsto 1$.

Curve Algorithm.

1. Choose $\Omega_\alpha = \sqcup_{i=1}^{2h} \omega_\alpha^i$ to be a pairwise disjoint collection of simple properly embedded arcs in $\Sigma_{h,3}$ with endpoints in ∂N_1 such that $\Sigma_{h,3} \setminus \Omega_\alpha$ is a pair of pants. Note that any such collection for $\Sigma_{h,3}$ must contain at least $2h$ arcs, so Ω_α is minimal.

2. Choose $\mathcal{C}_\alpha$, a simple properly embedded arc in $\Sigma_{h,3} \setminus \Omega_\alpha$ such that $\mathcal{C}_\alpha$ has endpoints c_α^1 in $\partial N_1 \setminus \partial\Omega_\alpha$ and c_α^2 in ∂N_2.

3. For each $1 \leq i \leq 2g+1$, define $\alpha_i = \{b_\gamma^i\} \times \partial N_3$.

4. For each $1 \leq j \leq 2h$ and each $1 \leq i \leq 2g+1$, define

$$\alpha_{(2g+1)j+i} = (\partial B_\alpha^i \times \omega_\alpha^j) \cup (B_\alpha^i \times \partial \omega_\alpha^j).$$

5. Define $\alpha_{(2g+1)(2h+1)+1} = (V \times \mathcal{C}_\alpha) \cup (B_\alpha \times \{c_\alpha^1\}) \cup (B_\beta \times \{c_\alpha^2\})$.

6. Repeat steps 1-5 with labels and indices permuted according to the permutation $(\alpha\beta\gamma)(123)$ to define Ω_β, $\mathcal{C}_\beta$, and $\boldsymbol{\beta} = (\beta_1, \ldots, \beta_{(2g+1)(2h+1)+1})$.

7. Repeat steps 1-5 with a second application of the permutation $(\alpha\beta\gamma)(123)$ to define Ω_γ, $\mathcal{C}_\gamma$, and $\boldsymbol{\gamma} = (\gamma_1, \ldots, \gamma_{(2g+1)(2h+1)+1})$.

Together with Σ, these $\boldsymbol{\alpha}$, $\boldsymbol{\beta}$, $\boldsymbol{\gamma}$ curves form our trisection diagram.

Proposition 3.11. *For each $1 \leq i \leq (2g+1)(2h+1)+1$ and $\delta \in \{\alpha, \beta, \gamma\}$, the curve δ_i defined by this algorithm is an essential simple closed curve in Σ.*

Proof. Recall that we may express the surface Σ as

$$\Sigma = (V \times \Sigma_{h,3}) \cup (B_\alpha \times \partial N_1) \cup (B_\beta \times \partial N_2) \cup (B_\gamma \times \partial N_3).$$

For each $1 \leq i \leq 2g+1$, the curve $\alpha_i = \{b_\gamma^i\} \times \partial N_3$ is boundary parallel in the annulus $B_\gamma^i \times \partial N_3$, and this annulus is essential in Σ by construction. Similarly, β_i and γ_i are core circles of the essential annuli $B_\alpha^i \times \partial N_1$ and $B_\beta^i \times \partial N_2$, respectively. Thus, each of these curves is itself essential in Σ.

For each $1 \leq j \leq 2h$ and each $1 \leq i \leq 2g+1$, note that ∂B_α^i is a set of two distinct points in Σ_g, and $\partial \omega_\alpha^j$ is a set of two distinct points in $\partial N_1 \subseteq \Sigma_{h,3}$. Hence, $\partial B_\alpha^i \times \omega_\alpha^j$ is a pair of disjoint arcs in $\partial B_\alpha \times \Sigma_{h,3}$, and $B_\alpha^i \times \partial \omega_\alpha^j$ is a pair of disjoint arcs in $B_\alpha \times \partial N_1$; the union of these four arcs is defined to be $\alpha_{(2g+1)j+i}$. As each of these four arcs is simple by design, and the intersection of $\partial B_\alpha^i \times \omega_\alpha^j$ and $B_\alpha^i \times \partial \omega_\alpha^j$ is the four point set $\partial B_\alpha^i \times \partial \omega_\alpha^j$, it follows that $\alpha_{(2g+1)j+i}$ is a simple closed curve in Σ. Furthermore, ω_α^j is essential in $\Sigma_{h,3}$ because Ω_α is minimal with respect to $\overline{\Sigma_{h,3} \setminus \Omega_\alpha}$ being a pair of pants. The essentiality of $\alpha_{(2g+1)j+i}$ in Σ follows, since we can find a loop in $\Sigma_{h,3}$ meeting ω_α^j, and hence $\alpha_{(2g+1)j+i}$, exactly once. Likewise, for each

$1 \leq j \leq 2h$ and $1 \leq i \leq 2g+1$, the curves $\beta_{(2g+1)j+i}$ and $\gamma_{(2g+1)j+i}$ are essential simple closed curves in Σ.

Finally, we consider the curve $\alpha_{(2g+1)(2h+1)+1} = (V \times \mathcal{C}_\alpha) \cup (B_\alpha \times \{c_\alpha^1\}) \cup (B_\beta \times \{c_\alpha^2\})$. Recall that V is a set of $4g+2$ distinct points (bounding each of B_α, B_β, and B_γ), and that $B_\alpha \cup B_\beta = \partial B_2$ in Σ_g, with $B_\alpha = \sqcup_{i=1}^{2g+1} B_\alpha^i$ and $B_\beta = \sqcup_{i=1}^{2g+1} B_\beta^i$. Enumerate $V = \{p_i\}_{i=1}^{4g+2}$ so that up to reordering (of B_α, B_β, and V), we have

$$\partial B_\alpha^i = \{p_{2i-1}, p_{2i}\}, \quad \partial B_\beta^i = \{p_{2i}, p_{2i+1}\}, \quad \text{and} \quad B_\alpha^i \cap B_\beta^j = \begin{cases} p_{2i} & \text{if } i = j \\ p_{2i-1} & \text{if } j = i-1 \\ \emptyset & \text{otherwise} \end{cases},$$

with indices taken mod $2g+1$. In other words, we may think of the boundary of B_2 as the loop $B_\alpha^1 B_\beta^1 B_\alpha^2 B_\beta^2 \cdots B_\alpha^{2g+1} B_\beta^{2g+1}$. Moreover, it is now evident that the path

$$(B_\alpha^1 \times \{c_\alpha^1\}) \bigcup_{(p_2, c_\alpha^1)} (\{p_2\} \times \mathcal{C}_\alpha) \bigcup_{(p_2, c_\alpha^2)} (B_\beta^1 \times \{c_\alpha^2\}) \bigcup_{(p_3, c_\alpha^2)} (\{p_3\} \times \mathcal{C}_\alpha) \cup \cdots$$
$$\cdots \cup (B_\beta^{2g+1} \times \{c_\alpha^2\}) \bigcup_{(p_1, c_\alpha^2)} (\{p_1\} \times \mathcal{C}_\alpha) \bigcup_{(p_1, c_\alpha^1)} (B_\alpha^1 \times \{c_\alpha^1\})$$

is a simple closed curve in Σ, but this is exactly $\alpha_{(2g+1)(2h+1)+1}$. A schematic of this path is shown in Figure 3.9.

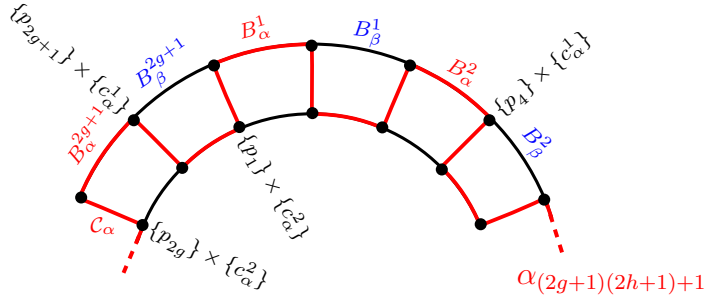

Figure 3.9: A schematic representation of the annulus $\partial B_2 \times \mathcal{C}_\alpha$, which contains the curve $\alpha_{(2g+1)(2h+1)+1}$.

To see that this curve is essential in Σ, note that it intersects the loop $\beta_1 =$

$\{b^1_\alpha\} \times \partial N_1$ exactly once, at the point $\{b^1_\alpha\} \times \{c^1_\alpha\}$. A similar argument establishes that $\beta_{(2g+1)(2h+1)+1}$ and $\gamma_{(2g+1)(2h+1)+1}$ also are essential simple closed curves in Σ. $\square$

Remark 3.12. The set of curves defined in step 4 of the curve algorithm may at first seem cluttered as we simultaneously define $(2h)(2g+1)$ curves. For a better understanding, we consider the effect of fixing each of our parameters i and j.

If we first fix i, say at $i = 1$, and look at the set $\{\alpha_{(2g+1)j+1} \mid 1 \leq j \leq 2h\}$, the algorithm defines this to be the set $\{(\partial B^1_\alpha \times \omega^j_\alpha) \cup (B^1_\alpha \times \partial\omega^j_\alpha) \mid 1 \leq j \leq 2h\}$. Equivalently, this is the set $(\{p_1\} \times \Omega_\alpha) \cup (\{p_2\} \times \Omega_\alpha) \cup (B^1_\alpha \times \partial\Omega_\alpha)$, using the enumeration of $V = \partial B_\alpha$ described in the proof of Proposition 3.11. In this set, we have $2h$ curves that each cross the annulus $B^i_\alpha \times \partial N_1$ exactly twice; in fact, this is all of the α curves that have this property. Remembering how Σ can be obtained from the 1-skeleton of our base surface, these $2h$ curves in Σ all correspond to the same unique edge (B^1_α) in that graph.

When we instead fix j, say at $j = 1$, we have the set $\{\alpha_{2g+1+i} \mid 1 \leq i \leq 2g+1\}$, which the algorithm defines as the set $\{(\partial B^i_\alpha \times \omega^1_\alpha) \cup (B^i_\alpha \times \partial\omega^1_\alpha) \mid 1 \leq i \leq 2g+1\}$. Alternatively, we may view this as the set $(V \times \omega^1_\alpha) \cup (B_\alpha \times \partial\omega^1_\alpha)$, a collection of $2g+1$ curves that each correspond to a different edge in the 1-skeleton of Σ_g, but which all share a copy of the arc ω^1_α in $\Sigma_{h,3}$. Thus, in some sense, fixing j gives us a single curve that is repeated along every edge in B_α.

Lemma 3.13. *The curve system $\boldsymbol{\alpha}$ (respectively $\boldsymbol{\beta}, \boldsymbol{\gamma}$) bounds a complete collection of disks in the 3-dimensional handlebody $X_1 \cap X_2$ (respectively $X_2 \cap X_3$, $X_3 \cap X_1$).*

Proof. Recall that from (3.2), (3.3), (3.5), we have

$$X_1 \cap X_2 = \left(B_\alpha \times \left(\overline{\Sigma_h \setminus (N_1 \sqcup N_2)}\right)\right) \cup (B_2 \times \partial N_2) \cup (B_\gamma \times N_3).$$

For $1 \leq i \leq 2g+1$, the curve $\alpha_i = \{b^i_\gamma\} \times \partial N_3$ bounds the disk $\{b^i_\gamma\} \times N_3$, which is a co-core of the 1-handle $B_\gamma \times N_3$ of $X_1 \cap X_2$. Moreover, from the proof of Lemma 3.5, we can see that compressing $X_1 \cap X_2$ along the curves $\{\alpha_i \mid 1 \leq i \leq 2g+1\}$ yields a genus $(2g+1)(2h)+1$ handlebody, which we will call H.

Now, for $1 \leq j \leq 2h$ and $1 \leq i \leq 2g+1$, the curve $\alpha_{(2g+1)j+i} = (\partial B^i_\alpha \times \omega^j_\alpha) \cup (B^i_\alpha \times \partial \omega^j_\alpha)$ bounds the disk $B^i_\alpha \times \omega^j_\alpha$, which is contained in $B_\alpha \times \left(\overline{\Sigma_h \setminus (N_1 \sqcup N_2)}\right)$. Furthermore, since $\Sigma_{h,3} \setminus \Omega_\alpha$ is a pair of pants, fixing $i \in \{1, \ldots, 2g+1\}$ and compressing H along the curves $\{\alpha_{(2g+1)j+i} \mid 1 \leq j \leq 2h\} = \partial(B^i_\alpha \times \Omega_\alpha)$ will reduce the genus of H by $2h$. Compressing H along all such curves thus yields a solid torus, which we will call T.

Finally, the curve $\alpha_{(2g+1)(2h+1)+1} = (V \times \mathcal{C}_\alpha) \cup (B_\alpha \times \{c^1_\alpha\}) \cup (B_\beta \times \{c^2_\alpha\})$ bounds the disk $(B_2 \times \{c^2_\alpha\}) \cup (B_\alpha \times \mathcal{C}_\alpha)$ as a subset of $(B_2 \times \partial N_2) \cup \left(B_\alpha \times \left(\overline{\Sigma_h \setminus (N_1 \sqcup N_2)}\right)\right)$; this disk is apparent in Figure 3.9. Since $\alpha_{(2g+1)(2h+1)+1}$ is essential in ∂T by construction, compressing T along $\alpha_{(2g+1)(2h+1)+1}$ yields a 3-ball. Hence, $\boldsymbol{\alpha}$ is a defining set of curves for $X_1 \cap X_2$. Similar arguments show that $\boldsymbol{\beta}$ defines $X_2 \cap X_3$, and $\boldsymbol{\gamma}$ defines $X_3 \cap X_1$. □

Corollary 3.14. $(\Sigma; \boldsymbol{\alpha}, \boldsymbol{\beta}, \boldsymbol{\gamma})$ *is a trisection diagram for* $X = \Sigma_g \times \Sigma_h$.

Example 3.15. We now trisect $T^2 \times S^2$, using the decomposition of T^2 given in Figure 3.1. The 1-skeleton of this decomposition is a trivalent graph on six vertices, giving us the genus 4 trisection surface shown in Figure 3.10.

Now, because $h = 0$, the surface $\Sigma_{0,3}$ is already a pair of pants, and thus $\Omega_\alpha = \Omega_\beta = \Omega_\gamma$ is empty, and steps 1 and 4 of the curve algorithm are trivial to implement. Additionally, up to isotopy there is a unique choice for each of $\mathcal{C}_\alpha$, $\mathcal{C}_\beta$, and $\mathcal{C}_\gamma$, depicted in Figure 3.11a. Now for $1 \leq i \leq 3$, we have $\alpha_i = \{b^i_\gamma\} \times \partial N_3$, $\beta_i = \{b^i_\alpha\} \times \partial N_1$, and $\gamma_i = \{b^i_\beta\} \times \partial N_2$; these curves are shown in Figure 3.11b. Our last three curves have the

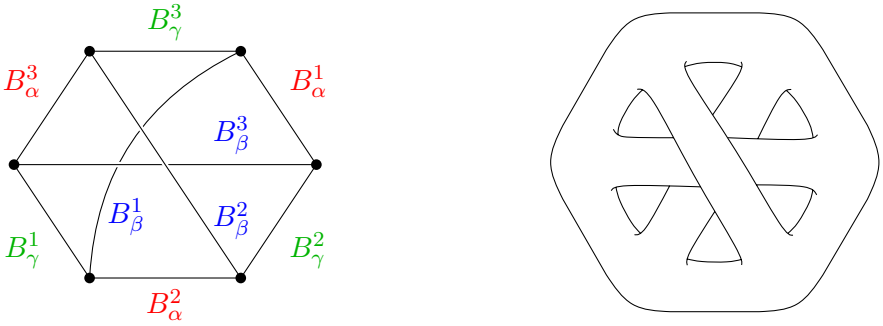

Figure 3.10: The 1-skeleton for T^2 and the corresponding trisection surface for $T^2 \times S^2$.

form $\alpha_4 = (V \times \mathcal{C}_\alpha) \cup (B_\alpha \times \{c^1_\alpha\}) \cup (B_\beta \times \{c^2_\alpha\})$, $\beta_4 = (V \times \mathcal{C}_\beta) \cup (B_\beta \times \{c^1_\beta\}) \cup (B_\gamma \times \{c^2_\beta\})$, and $\gamma_4 = (V \times \mathcal{C}_\alpha) \cup (B_\gamma \times \{c^1_\gamma\}) \cup (B_\alpha \times \{c^2_\gamma\})$ (see Figure 3.11c). The full trisection diagram is shown in Figure 3.12.

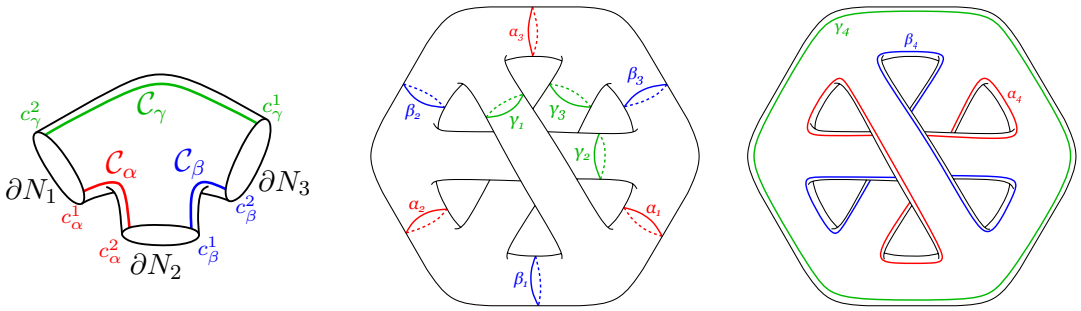

(a) (b) (c)

Figure 3.11: Curve placement on Σ, a trisection surface for $T^2 \times S^2$.

Remark 3.16. The trisection diagrams in Figures 3.8 and 3.12 are related by a surface diffeomorphism and a sequence of handle slides, indicating that this is in fact the same trisection of $X = T^2 \times S^2$. Figure 3.13 shows a trisection diagram that is handle-slide equivalent to the diagram for $S^2 \times T^2$ constructed in Example 3.9, and related to the diagram for $T^2 \times S^2$ constructed in Example 3.15 by the surface

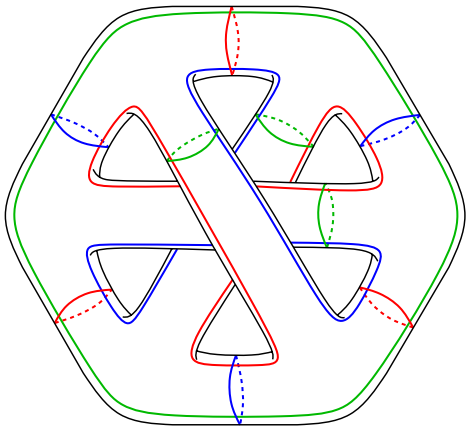

Figure 3.12: A trisection diagram for $T^2 \times S^2$.

diffeomorphism that takes the curve triple $(\alpha_1, \beta_1, \gamma_1)$ in Figure 3.8 to the curve triple $(\alpha_4, \beta_4, \gamma_4)$ in Figure 3.12.

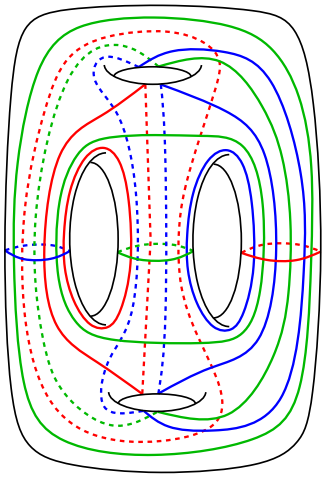

Figure 3.13: Another trisection diagram for $S^2 \times T^2$. A sequence of handle slides will transform this diagram to that in Figure 3.8, and a surface diffeomorphism will transform this diagram to that in Figure 3.12.

3.3 Minimality

In this section, we prove that the trisection of $\Sigma_g \times \Sigma_h$ defined in Section 3.1 is minimal. Our proof leverages the fact that a trisection of a 4-manifold X induces a handle decomposition of X, which then corresponds to a presentation of $\pi_1(X)$. In particular, Gay and Kirby showed that a 4-manifold admitting an (ℓ, k)-trisection also admits a handle decomposition with one 0-handle, k 1-handles, $\ell - k$ 2-handles, k 3-handles, and one 4-handle [GK16, Theorem 4]. A more general statement, for possibly unbalanced trisections, says that a 4-manifold with an $(\ell; k_1, k_2, k_3)$-trisection admits a handle decomposition with one 0-handle, k_1 1-handles, $\ell - k_2$ 2-handles, k_3 3-handles, and one 4-handle [MSZ16]. Furthermore, the symmetry of a trisection invokes a triality among the sectors, in which permuting X_1, X_2, and X_3 still produces a trisection. Thus, there is a corresponding triality of handles in a handle decomposition of a trisected 4-manifold. Recall from Section 2.1 that a handle decomposition gives rise to a cell structure on X in which k-handles correspond to k-cells, and that the 1- and 2-cells of a cell complex X determine a presentation for $\pi_1(X)$. It follows that the number of 1-handles in a handle decomposition of X is bounded below by the rank of $\pi_1(X)$. This leads us to the following theorem:

Theorem 3.17. *The trisection genus of $X^4 = \Sigma_g \times \Sigma_h$ is $(2g+1)(2h+1)+1$. That is, the $((2g+1)(2h+1)+1; 2g+2h)$-trisection of X^4 constructed in Theorem 3.3 is minimal.*

Proof. Let F^n denote the free group of rank n. For some relator sets R_1, R_2, R_3, note that

$$\pi_1(\Sigma_g \times \Sigma_h) \cong \pi_1(\Sigma_g) \times \pi_1(\Sigma_h) \cong (F^{2g}/\langle R_1 \rangle^N) \times (F^{2h}/\langle R_2 \rangle^N) \cong F^{2g+2h}/\langle R_3 \rangle^N$$

has rank $2g+2h$. Thus, trisection triality grants that $\min\{k_1, k_2, k_3\} \geq 2g+2h$ for any $(\ell; k_1, k_2, k_3)$-trisection of $X^4 = \Sigma_g \times \Sigma_h$. In particular, when $k_1 = k_2 = k_3 = 2g + 2h$, such a trisection cannot be destabilized, as doing so would reduce one of the k_i's by one. Finally, since the Euler characteristic, χ, of X is $\chi = 2 + \ell - \sum_{i=1}^{3} k_i$, it follows that ℓ is minimal when $\sum_{i=1}^{3} k_i$ is minimal. Therefore, the trisection genus of $\Sigma_g \times \Sigma_h$ is at least $(2g + 1)(2h + 1) + 1$, and this is achieved precisely with Theorem 3.3. $\square$

CHAPTER 4

TRISECTING FLAT SURFACE BUNDLES OVER SURFACES

The purpose of this chapter is to generalize Theorem 3.3 to trisections of flat surface bundles over surfaces with orientable fibers and orientable or non-orientable bases. We do this in Section 4.1. In Section 4.2, we present an algorithm to construct trisection diagrams for a special case of flat surface bundles with both base and fiber orientable, and conjecture that only a slight modification of the algorithm is necessary for general flat bundles. The chapter concludes with a proof in Section 4.3 that the diagram from the algorithm corresponds to the trisection given in Theorem 4.3.

Throughout this chapter, we let $F_n = \#^n \mathbb{RP}^2$ denote the closed, connected, non-orientable surface of genus n. Let S in $\{\Sigma_g, F_k \mid g \geq 0, k \geq 1\}$ be given, and let χ denote the Euler characteristic of S; recall $\chi(\Sigma_g) = 2 - 2g$ and $\chi(F_k) = 2 - k$.

Lemma 4.1. *S admits a cell structure consisting of $6-2\chi$ vertices, $9-3\chi$ edges, and three faces. In particular, we may write $S = B_1 \cup B_2 \cup B_3$, subject to the following:*

- *Each B_i is diffeomorphic to a closed 2-disk B^2.*
- *The pairwise intersections of these disks are $B_\alpha = B_1 \cap B_2$, $B_\beta = B_2 \cap B_3$, and $B_\gamma = B_3 \cap B_1$; each is a pairwise disjoint collection of $3 - \chi$ edges and may be*

enumerated as $B_\alpha = \sqcup_{i=1}^{3-\chi} B_\alpha^i$, *etc.*

- *The triple intersection* $B_1 \cap B_2 \cap B_3 = \partial B_\alpha = \partial B_\beta = \partial B_\gamma$ *is a disjoint union of* $6 - 2\chi$ *vertices. We call this set* V.

Proof. When $S = \Sigma_g$ is orientable, this is the same decomposition described in Lemma 3.1 and used throughout Chapter 3. We remind the reader that in this case, Figure 3.1 depicts an appropriate decomposition of S. In the case where $S = F_k$ is non-orientable, the decomposition shown in Figure 4.1 suffices, with the connect sum taken at an appropriate pair of vertices (similar to Figure 3.2). □

Remark 4.2. The constructions that follow will always use this decomposition for $S = F_k$, and the decomposition in Figure 3.1 for $S = \Sigma_g$.

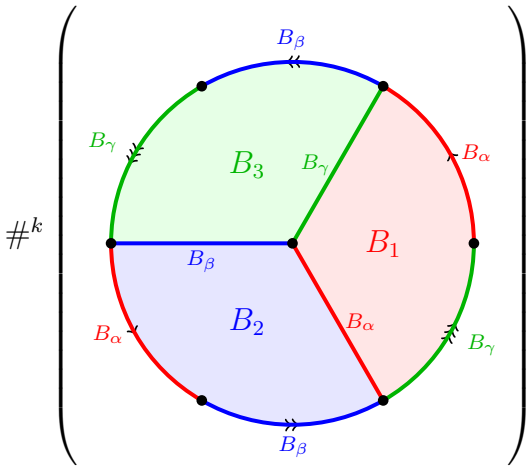

Figure 4.1: A disk decomposition of the base surface $F_k = \#^k \mathbb{RP}^2$

Fix $h \geq 0$, and let X^4 be an orientable Σ_h-bundle over S with monodromy representation $\varphi : \pi_1(S) \to \mathrm{MCG}^{\pm}(\Sigma_h)$; recall that such a bundle is called *flat* when the monodromy representation lifts to a map $\tilde{\varphi} : \pi_1(S) \to \mathrm{Diff}(\Sigma_h)$ so that $\pi \circ \tilde{\varphi} = \varphi$, where $\pi : \mathrm{Diff}(\Sigma_h) \to \mathrm{MCG}^{\pm}(\Sigma_h)$ is the quotient map. In particular, we assume

$\tilde{\varphi} : \pi_1(S) \to \mathrm{Diff}(\Sigma_h)$ is a lift of φ such that X can be obtained in the following way: To each edge in the 1-skeleton of S, assign a choice of transverse direction. Let $x_0 \in V$ be chosen so that, up to relabeling, the edges adjacent to x_0 are $B_\alpha^{3-\chi}$, $B_\beta^{3-\chi}$, and $B_\gamma^{3-\chi}$. Now, let D be the disk obtained by starting with the disk B_1, attaching B_2 by identification along the edge $B_\alpha^{3-\chi}$, and then attaching B_3 by identification along the edges $B_\beta^{3-\chi} \cup B_\gamma^{3-\chi}$. We now have S as the quotient of D, a $(12-6\chi)$-gon, by pairwise edge identification. For each $\delta \in \{\alpha, \beta, \gamma\}$, for each $1 \leq i \leq 2-\chi$, let t_δ^i be the element of $\pi_1(S, x_0)$ that starts at x_0, runs in the interior of D to the middle of the edge B_δ^i, crosses the edge in the indicated transverse direction, and returns in the interior of D back to x_0. Thus, we can label each edge of ∂D with a diffeomorphism $\tilde{\varphi}(t_\delta^i)$ and a transverse direction, and obtain X from $D \times \Sigma_h$ by identifying the two copies of $B_\delta^i \times \Sigma_h$ via the labeling, for each $1 \leq i \leq 2-\chi$ and $\delta \in \{\alpha, \beta, \gamma\}$. We denote this bundle structure by $X = S \times_{\tilde{\varphi}} \Sigma_h$. Conjecturally, every surface bundle has this structure (see [MT19]).

4.1 A trisection of $S \times_{\tilde{\varphi}} \Sigma_h$

In this section, we use the flat structure on $X = S \times_{\tilde{\varphi}} \Sigma_h$ to define and prove a trisection of X. We then show that this trisection is minimal in certain cases.

Let $p : X \to S$ be the fibration, and choose disjoint sections σ_1, σ_2, and σ_3 over B_1, B_2, and B_3, respectively. Let ν_i be a closed tubular neighborhood of σ_i for $i = 1, 2, 3$, with the ν_i's also disjoint. The flat structure of X discussed above allows each section σ_i to have the form $B_i \times \{q_i\} \subset D \times \Sigma_h$ for some point q_i in the fiber Σ_h, by choosing q_i such that the sets $\{q_i, \tilde{\varphi}(t_\delta^j)(q_i) \mid 1 \leq j \leq 2-\chi\}$ are distinct for $1 \leq i \leq 3$. Furthermore, each neighborhood ν_i has the form $B_i \times N_i \subset D \times \Sigma_h$, where N_i is a closed tubular neighborhood of q_i in Σ_h; we will be heavily relying on this structure

throughout this section. With indices taken mod 3, define

$$X_i = \overline{p^{-1}(B_i) \setminus \nu_i} \cup \nu_{i+1} \tag{4.1}$$

for $i = 1, 2, 3$. Note that this definition agrees with (3.1) when $X = \Sigma_g \times \Sigma_h$.

Theorem 4.3. *With X_1, X_2, X_3 defined as in (4.1), let $\Sigma := X_1 \cap X_2 \cap X_3$. Then $(\Sigma; X_1, X_2, X_3)$ is a $((3-\chi)(2h+1)+1; 2-\chi+2h)$-balanced trisection of $X = S \times_{\tilde{\varphi}} \Sigma_h$.*

Before proving Theorem 4.3 in full, we first address the nature of the pairwise and triple intersections among the X_i with Lemmas 4.4 and 4.5. The arguments presented here are similar to those presented in Chapter 3, but have been adapted to accommodate the nontrivial bundle structure.

Lemma 4.4. *For each pair $1 \leq i \neq j \leq 3$, the intersection $X_i \cap X_j$ is a 3-dimensional handlebody with genus $(3-\chi)(2h+1)+1$.*

Proof. The 3-dimensional intersection of $X_1 \cap X_2$ is the union of four pieces:

(a) The first piece, $\overline{p^{-1}(B_1) \setminus \nu_1} \cap \overline{p^{-1}(B_2) \setminus \nu_2}$, is $3-\chi$ copies of a genus $2h+1$ handlebody. In particular, since the sections σ_i and their neighborhoods ν_i were chosen to be disjoint, this intersection is diffeomorphic to $B_\alpha \times \Sigma_{h,2}$ using the local coordinates on either $p^{-1}(B_1)$ or $p^{-1}(B_2)$. With $\Sigma_{h,2}$ having two boundary components, thickening a copy of this surface yields a genus $2h+1$ 3-dimensional handlebody; there are $3-\chi$ such handlebodies here because B_α has $3-\chi$ connected components.

(b) The second piece, $\nu_2 \cap \overline{p^{-1}(B_2) \setminus \nu_2} = \partial\nu_2$ is a solid torus, diffeomorphic to $B_2 \times \partial N_2$ using the local coordinates on $p^{-1}(B_2)$. The torus boundary of this

piece is $\partial B_2 \times \partial N_2 = (B_\alpha \times \partial N_2) \cup (B_\beta \times \partial N_2)$, which intersects the ith component of the previous piece in the annulus $B^i_\alpha \times \partial N_2$.

Thus, attaching $\overline{p^{-1}(B_1) \setminus \nu_1} \cap \overline{p^{-1}(B_2) \setminus \nu_2}$ to $\nu_2 \cap \overline{p^{-1}(B_2) \setminus \nu_2}$ involves stacking up the $3 - \chi$ different handlebodies so that one solid torus summand of each lines up. It follows that $X_1 \cap \overline{p^{-1}(B_2) \setminus \nu_2}$ is connected, and is a 3-dimensional handlebody with genus $(3 - \chi)(2h) + 1$.

(c) The third piece, $\overline{p^{-1}(B_1) \setminus \nu_1} \cap \nu_3$, is a collection of $3-\chi$ pairwise disjoint 3-balls, each diffeomorphic to $B^i_\gamma \times N_3$ for some $1 \leq i \leq 3-\chi$. Since B_α and B_γ intersect only on their common boundary, V, it follows that each component $B^i_\gamma \times N_3$ is attached to $X_1 \cap \overline{p^{-1}(B_2) \setminus \nu_2}$ along the two disks comprising $\partial B^i_\gamma \times N_3$ sitting in the boundary of $B_\alpha \times \Sigma_{h,2} \subset p^{-1}(B_1)$. Thus, this piece contributes $3 - \chi$ 1-handles.

(d) The final piece, $\nu_2 \cap \nu_3$, is empty by construction.

Therefore, $X_1 \cap X_2$ is a 3-dimensional handlebody with genus $(3 - \chi)(2h + 1) + 1$. A permutation of indices in the preceding argument produces the same result for $X_2 \cap X_3$ and $X_3 \cap X_1$, since each may be viewed as $X_i \cap X_{i+1}$ for some choice of i. $\square$

As in Remark 3.6, the form of the triple intersection $X_1 \cap X_2 \cap X_3$ follows from the other conditions on the X_i, but the analysis presented in the proof of Lemma 4.5 is useful in the discussion of the generalized curve algorithm in the next section.

Lemma 4.5. *Let X_1, X_2, X_3 be defined as in* (4.1)*, and define $\Sigma := X_1 \cap X_2 \cap X_3$ as their triple intersection. Then Σ is diffeomorphic to $\Sigma_{(3-\chi)(2h+1)+1}$.*

Proof. The proof of Lemma 4.4 describes $X_1 \cap X_2$ as the union of a subset of $p^{-1}(\partial B_1) = p^{-1}(B_\gamma \cup B_\alpha)$ and a subset of $p^{-1}(B_2)$. Symmetry with the other pairwise intersections grants that the triple intersection $\Sigma = X_1 \cap X_2 \cap X_3$ is a subset

of $p^{-1}(B_\gamma \cup B_\alpha \cup B_\beta)$; in what follows, we consider Σ relative to the local product structure of $p^{-1}(B_1) \supset p^{-1}(B_\gamma \cup B_\alpha)$. In particular, building off of the previous proof, we have Σ as the union of the following four pieces; the labels here correspond to those used in the proof of Lemma 4.4:

(a1) $\left[\overline{p^{-1}(B_1) \setminus \nu_1} \cap \overline{p^{-1}(B_2) \setminus \nu_2}\right] \cap \overline{p^{-1}(B_3) \setminus \nu_3}$ is diffeomorphic to $V \times \Sigma_{h,3}$, a collection of $2(3-\chi)$ copies of $\Sigma_{h,3}$.

(a2) $\left[\overline{p^{-1}(B_1) \setminus \nu_1} \cap \overline{p^{-1}(B_2) \setminus \nu_2}\right] \cap \nu_1$ is diffeomorphic to $B_\alpha \times \partial N_1$. Each component $B_\alpha^i \times \partial N_1$ has two boundary components, which coincide with two boundary components of the disconnected surface in (a1). Gluing these together connects the copies of $\Sigma_{h,3}$ in pairs, yielding a collection of $3-\chi$ copies $\Sigma_{2h,4}$.

(c) $\left[\overline{p^{-1}(B_1) \setminus \nu_1} \cap \nu_3\right] \cap \overline{p^{-1}(B_3) \setminus \nu_3}$ is diffeomorphic to $B_\gamma \times \partial N_3$. Again, each component $B_\gamma^i \times \partial N_3$ has two boundary components, which each coincide with a boundary component of the surface we have constructed so far. Attaching these annuli produces a copy of $\Sigma_{(3-\chi)(2h)+1,2(3-\chi)}$, where each of the remaining boundary components corresponds to $\{v\} \times \partial N_2$ for some $v \in V$. This surface is entirely contained in the trivial bundle $p^{-1}(\partial B_1) \cong B_1 \times \Sigma_h$.

(b) $\partial\nu_2 \cap X_3 = \partial\nu_2 \cap p^{-1}(B_3) \setminus \nu_3$ is diffeomorphic to $B_\beta \times \partial N_2$ as a subset of $p^{-1}(B_\beta)$.

This final piece is glued to our surface via some diffeomorphisms of the S^1 boundary components that preserve orientability of the total surface. Thus, we are left with Σ as diffeomorphic to $\Sigma_{(3-\chi)(2h+1)+1}$. Additionally, this breakdown of Σ into pieces makes it readily recognizable as the boundary of each 3-dimensional handlebody $X_i \cap X_{i+1}$. $\square$

Proof of Theorem 4.3. We first note that $\overline{p^{-1}(B_i) \setminus \nu_i}$ is diffeomorphic to $B_i \times \overline{\Sigma_h \setminus N_i}$, a 4-dimensional 1-handlebody with genus $2h$. Since the intersection of this with ν_{i+1} is

$3-\chi$ mutually disjoint 3-balls, we may glue ν_{i+1} to $\overline{p^{-1}(B_i) \setminus \nu_i}$ by attaching at each 3-ball one at a time. This amounts to adding $3-\chi$ 1-handles, the first of which connects ν_{i+1} with $\overline{p^{-1}(B_i) \setminus \nu_i}$, while the remaining $2-\chi$ handles add to the genus. Thus, each X_i is a 4-dimensional 1-handlebody with genus $2-\chi+2h$. Lemmas 4.4 and 4.5 established that the pairwise and triple intersections of these pieces are 3-dimensional handlebodies and a surface, respectfully, each with genus $(3-\chi)(2h+1)+1$.

The fact that $X = X_1 \cup X_2 \cup X_3$ is immediate from the definition of the X_i. Moreover, as in the trivial bundle case, Lemma 3.8 yields that for each $1 \leq i \leq 3$, we have $X_i \cap X_{i+1} = \partial X_i \cap \partial X_{i+1}$, and $\Sigma = \partial(X_i \cap X_{i+1})$. This completes the proof. □

Proposition 4.6. *Let X be as in Theorem 4.3. If $\pi_1(X)$ has rank $2-\chi+2h$, then the trisection genus of X is $(3-\chi)(2h+1)+1$.*

Proof. The proof of Theorem 3.17 carries over directly. □

Remark 4.7. The topic of minimality is revisited in Section 5.2 with a discussion of how Proposition 4.6 might be strengthened, and how the trisection genus of a flat surface bundle over a surface might be calculated in general.

4.2 A diagram algorithm for certain flat bundles

In this section, we present an algorithm for constructing a trisection diagram for a flat Σ_h-bundle over Σ_g in the case where the associated diffeomorphisms $\tilde{\varphi}(\cdot)$ each fix a handful of points (see Remark 4.9). We begin with a particular description of the base, the details of which require that that surface be orientable. We then state the diagram algorithm, which takes this description of the base together with the flat bundle structure encoded by $\tilde{\varphi}$, and outputs three systems of curves in Σ. In the algorithm statement, we highlight those parts that are the same as for the trivial

bundles discussed in Section 3.2. The section is wrapped up with an example of the algorithm for a T^2-bundle over T^2. The proof that the algorithm gives a diagram corresponding to the trisection from Section 4.1 is deferred until Section 4.3.

Remark 4.8. Despite focusing on the case where the base is the orientable surface Σ_g, we continue to use χ, the Euler characteristic of the base, as a parameter in our arguments, rather than g. This fits more naturally with the proofs of Section 4.1, and the algorithm conjecturally extends to bundles with non-orientable base; this extension is more easily seen in terms of χ. That being said, the similarities with the algorithm in Chapter 3 are more easily recognized by substituting $2-2g$ for each instance of χ in what follows.

To each edge in the 1-skeleton of Σ_g, assign an orientation and a consistent choice of transverse direction according to the right-hand rule, as shown in Figure 4.2. For convenience, we orient edges so that the boundaries of B_1 and B_3 each have a coherent orientation, with transverse directions (for B_γ and B_α) all pointing to the interior of B_1, and transverse directions (for B_β and B_γ) all pointing outward from B_3. Additionally, enumerate the vertex set V as $\{p_1, p_2, \ldots, p_{6-2\chi}\}$, with vertex order following the chosen orientation of ∂B_3 such that $p_{5-2\chi}$ is the basepoint x_0 defined at the start of this chapter. Relabel, if necessary, the edges $\{B^i_\alpha, B^i_\beta, B^i_\gamma \mid 1 \leq i \leq 3-\chi\}$ so that the boundary of B_3 based at x_0 is the oriented path

$$B^{3-\chi}_\gamma, B^1_\beta, B^1_\gamma, \ldots, B^{2-\chi}_\beta, B^{2-\chi}_\gamma, B^{3-\chi}_\beta, \tag{4.2}$$

and the boundary of B_1 based at x_0 is the oriented path

$$B^{k_3-\chi}_\gamma, B^1_\alpha, B^{k_1}_\gamma, \ldots, B^{2-\chi}_\alpha, B^{k_2-\chi}_\gamma, B^{3-\chi}_\alpha, \tag{4.3}$$

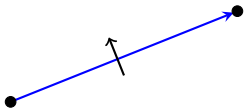

Figure 4.2: An oriented edge (in blue) and the associated transverse direction (in black)

for some ordering $k_1, \ldots, k_{3-\chi}$ of the set $\{1, \ldots, 3-\chi\}$. Note that we necessarily have $k_{3-\chi} = 3-\chi$, as x_0 is the common endpoint of the edges $B_\alpha^{3-\chi}, B_\beta^{3-\chi}, B_\gamma^{3-\chi}$. Finally, note that for each $1 \leq i \leq 3-\chi$, and with indices taken mod $6-2\chi$ as needed, we have: the edge B_α^i starts at p_{2k_i-1} and ends at p_{2k_i-1}; the edge B_β^i starts at p_{2i-2} and ends at p_{2i-1}; the edge B_γ^i starts at p_{2i-1} and ends at p_{2i}; the loop t_α^i crosses the edge B_α^i from B_2 into B_1; the loop t_β^i crosses the edge B_β^i from B_3 into B_2; the loop t_γ^i crosses the edge B_γ^i from B_3 into B_1. Here, the loops t_δ^i, for $\delta \in \{\alpha, \beta, \gamma\}$ and $1 \leq i \leq 2-\chi$, are as defined at the start of Chapter 4, and we define the loops $t_\delta^{3-\chi}$ to be trivial in $\pi_1(\Sigma_g, x_0)$. See Figure 4.3a for a depiction of these orientations and labels in the case where $g = 1$.

Remark 4.9. The following algorithm requires that each map $\tilde{\varphi}(t_\beta^i)$ fixes $\partial\Omega_\beta \cup \partial\mathcal{C}_\beta$ pointwise, and that each map $\tilde{\varphi}(t_\alpha^i)$ fixes $\partial\Omega_\gamma \cup \partial\mathcal{C}_\gamma$ pointwise, where these sets are defined in steps 1 and 2 of the algorithm. This occurs, for instance, when the images of the standard generators for $\pi_1(\Sigma_g)$ under $\tilde{\phi}$ have small support, as with products of Dehn twists about disjoint simple closed curves.

Generalized Curve Algorithm. Steps 1–3 of this algorithm define the same arcs and curves as appear in Section 3.2. Additionally, the $\boldsymbol{\alpha}$ curves defined in steps 4–5 are the same.

1. a) Choose $\Omega_\alpha = \sqcup_{i=1}^{2h} \omega_\alpha^i$ to be a pairwise disjoint collection of simple properly embedded arcs in $\Sigma_{h,3}$ with endpoints in ∂N_1 such that $\Sigma_{h,3} \setminus \Omega_\alpha$ is a pair

of pants. As in Section 3.2, Ω_α is minimal.

b) Choose $\Omega_\beta = \sqcup_{i=1}^{2h} \omega_\beta^i$ to be a pairwise disjoint collection of simple properly embedded arcs in $\Sigma_{h,3}$ with endpoints in ∂N_2 such that $\Sigma_{h,3} \setminus \Omega_\beta$ is a pair of pants.

c) Choose $\Omega_\gamma = \sqcup_{i=1}^{2h} \omega_\gamma^i$ to be a pairwise disjoint collection of simple properly embedded arcs in $\Sigma_{h,3}$ with endpoints in ∂N_3 such that $\Sigma_{h,3} \setminus \Omega_\gamma$ is a pair of pants.

2. a) Choose $\mathcal{C}_\alpha$, a simple properly embedded arc in $\Sigma_{h,3} \setminus \Omega_\alpha$ such that $\mathcal{C}_\alpha$ has endpoints c_α^1 in $\partial N_1 \setminus \partial\Omega_\alpha$ and c_α^2 in ∂N_2.

b) Choose $\mathcal{C}_\beta$, a simple properly embedded arc in $\Sigma_{h,3} \setminus \Omega_\beta$ such that $\mathcal{C}_\beta$ has endpoints c_β^1 in $\partial N_2 \setminus \partial\Omega_\beta$ and c_β^2 in ∂N_3.

c) Choose $\mathcal{C}_\gamma$, a simple properly embedded arc in $\Sigma_{h,3} \setminus \Omega_\gamma$ such that $\mathcal{C}_\gamma$ has endpoints c_γ^1 in $\partial N_3 \setminus \partial\Omega_\gamma$ and c_γ^2 in ∂N_1.

3. For each $1 \leq i \leq 3 - \chi$, let b_δ^i denote the midpoint of the edge B_δ^i for each $\delta \in \{\alpha, \beta, \gamma\}$. Additionally, define:

$$\alpha_i = \{b_\gamma^i\} \times \partial N_3 \qquad \beta_i = \{b_\alpha^i\} \times \partial N_1 \qquad \gamma_i = \{b_\beta^i\} \times \partial N_2$$

4. For each $1 \leq j \leq 2h$ and each $1 \leq i \leq 3 - \chi$, let $\overline{t_\alpha^i}$ denote the reverse of the loop t_α^i, and define:

$$\alpha_{(3-\chi)j+i} = (\partial B_\alpha^i \times \omega_\alpha^j) \cup (B_\alpha^i \times \partial\omega_\alpha^j)$$
$$\beta_{(3-\chi)j+i} = \left(\partial B_\beta^i \times \tilde{\varphi}(t_\beta^i)(\omega_\beta^j)\right) \cup (B_\beta^i \times \partial\omega_\beta^j)$$
$$\gamma_{(3-\chi)j+i} = \left(\{p_{2k_i-1}\} \times \tilde{\varphi}(\overline{t_\alpha^i})(\omega_\gamma^j)\right) \cup \left(B_\gamma^{k_i} \times \partial\omega_\gamma^j\right) \cup \left(\{p_{2k_i}\} \times \tilde{\varphi}(\overline{t_\alpha^{i+1}})(\omega_\gamma^j)\right)$$

5. Finally, define:

$$\alpha_{(3-\chi)(2h+1)+1} = (\partial B_\alpha \times \mathcal{C}_\alpha) \cup (B_\alpha \times \{c_\alpha^1\}) \cup (B_\beta \times \{c_\alpha^2\})$$

$$\beta_{(3-\chi)(2h+1)+1} = \sqcup_{i=1}^{3-\chi} \left(\partial B_\beta^i \times \tilde{\varphi}(t_\beta^i)(\mathcal{C}_\beta)\right) \cup (B_\beta \times \{c_\beta^1\}) \cup (B_\gamma \times \{c_\beta^2\})$$

$$\gamma_{(3-\chi)(2h+1)+1} = \sqcup_{i=1}^{3-\chi} \left(\partial B_\alpha^i \times \tilde{\varphi}(\overline{t_\alpha^i})(\mathcal{C}_\gamma)\right) \cup (B_\gamma \times \{c_\gamma^1\}) \cup (B_\alpha \times \{c_\gamma^2\})$$

Together with Σ, these $\boldsymbol{\alpha}$, $\boldsymbol{\beta}$, $\boldsymbol{\gamma}$ curves form our trisection diagram.

Conjecture 4.10. *A slightly more general description of the curves defined in the algorithm should yield an extension to bundles with non-orientable base, and to bundles where the points specified in Remark 4.9 need not be fixed by the specified maps.*

Example 4.11. In this example, we demonstrate the algorithm with a particular T^2-bundle over T^2. To define the bundle, we first need a map $\tilde{\varphi} : \pi_1(\text{base}) \to \text{Diff}(\text{fiber})$, which we define using the presentation $\pi_1(T^2, x_0) = \langle a, b \mid aba^{-1}b^{-1} \rangle$ and Dehn twists about the curves $\ell, \mu \in T^2$ (see Figure 4.3).

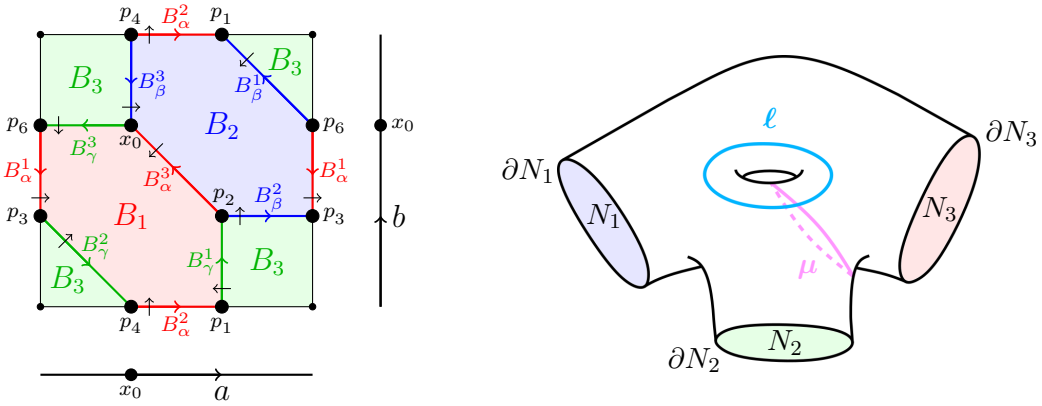

(a) The base, T^2, with $\pi_1(T^2, x_0) = \langle a, b \rangle$ (b) The fiber, T^2, with $\tau_{\mu\ell} \in \text{Diff}(T^2)$

Figure 4.3: The structures imposed on the base and fiber surfaces of $T^2 \times_{\tilde{\varphi}} T^2$

Notation. We use τ_c to denote a right Dehn twist about a curve c, so that τ_c^{-1} denotes a left Dehn twist about c. Additionally, we use τ_{cd} to mean τ_c followed by τ_d. Figure 4.4 depicts $\tau_\ell(T^2)$.

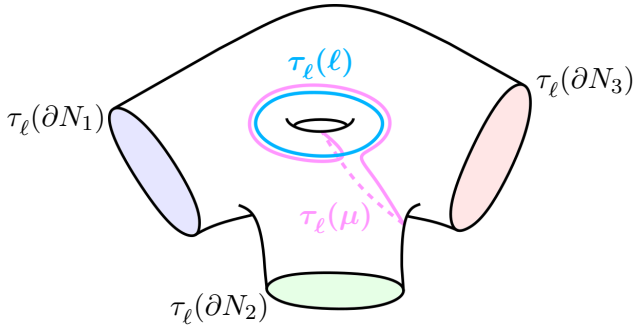

Figure 4.4: The result of applying τ_ℓ to the fiber surface

The particular bundle we are working with is $T^2 \times_{\tilde{\varphi}} T^2$, where $\tilde{\varphi} : \langle a, b \rangle \to \mathrm{Diff}(T^2)$ is given by $\tilde{\varphi}(a) = \tau_{\mu\ell}$ and $\tilde{\varphi}(b) = (\tau_{\mu\ell})^{-1}$. The arcs chosen in steps 1 and 2 of the algorithm are shown in Figure 4.5. Note that Ω_α and $\mathcal{C}_\alpha$ are the same as in Figure 3.7a, from the trisection of $S^2 \times T^2$.

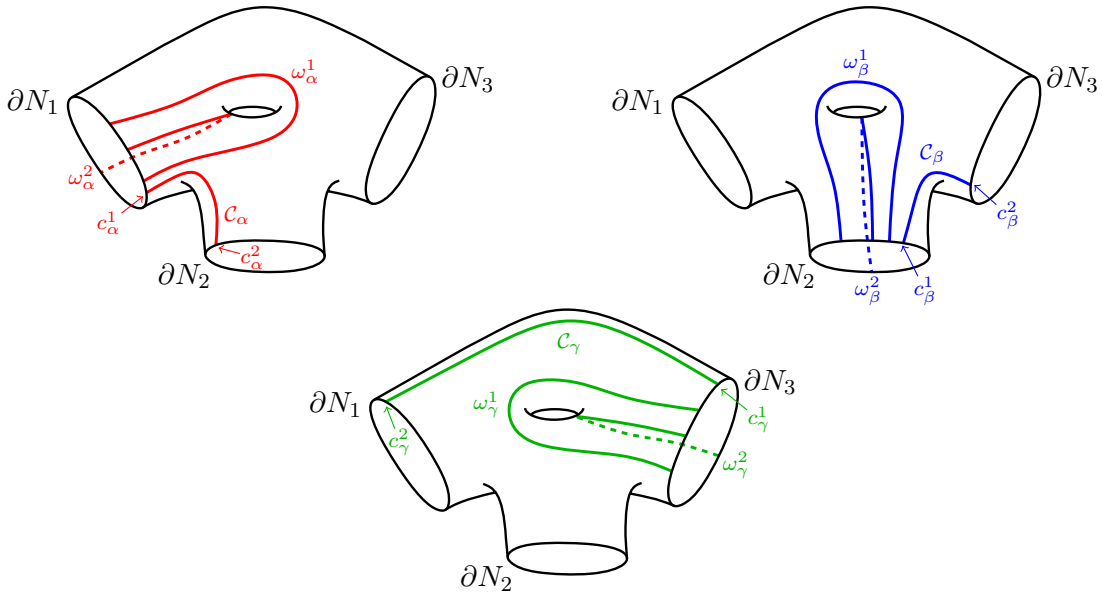

Figure 4.5: Arcs in $\Sigma_{1,3}$

Steps 4 and 5 of the algorithm involve images of these arcs under different diffeomorphisms of the fiber surface, and it will be helpful to have those images before we

draw the full diagram. In particular, we need to know how to write the loops t_δ^i as elements of $\langle a, b\rangle$, for $\delta \in \{\alpha, \beta\}$ and $1 \leq i \leq 3$. From Figure 4.3a, we observe:

$$t_\alpha^1 = a, \qquad t_\alpha^2 = b, \qquad t_\alpha^3 = 1, \qquad t_\beta^1 = a^{-1}, \qquad t_\beta^2 = a^{-1}b, \qquad t_\beta^3 = 1, \tag{4.4}$$

as elements of $\pi_1(T^2, x_0)$. Additionally, from the boundary path of B_1 we see that $B_\gamma^{k_1} = B_\gamma^2$, $B_\gamma^{k_2} = B_\gamma^1$, and $B_\gamma^{k_3} = B_\gamma^3$. We now have the tools to draw the more complicated pieces of the curves in steps 4–5. Beginning with the $\boldsymbol{\beta}$ curves, recall that for $1 \leq j \leq 2$ and $1 \leq i \leq 3$ we have the arcs $\partial B_\beta^i \times \tilde{\varphi}(t_\beta^i)(\omega_\beta^j)$ contained in β_{3j+i}. Furthermore, β_{10} contains the arcs $\sqcup_{i=1}^{3-\chi} \left(\partial B_\beta^i \times \tilde{\varphi}(t_\beta^i)(\mathcal{C}_\beta)\right)$. From (4.4) and the definition of $\tilde{\varphi}$, we know that $\tilde{\varphi}(t_\beta^1) = (\tau_{\mu\ell})^{-1}$, $\tilde{\varphi}(t_\beta^2) = (\tau_{\mu\ell})^{-2}$, and $\tilde{\varphi}(t_\beta^3) = 1$. Note that for each i, the two components of $\partial B_\beta^i \times \Sigma_{h,3}$ look the same with regards to the $\boldsymbol{\beta}$ curves, so we need only consider three cases. Figure 4.6 shows $\tilde{\varphi}(t_\beta^i)(\mathcal{C}_\beta \cup \Omega_\beta)$ for each $1 \leq i \leq 3$, with each arc labeled according to which curve contains it.

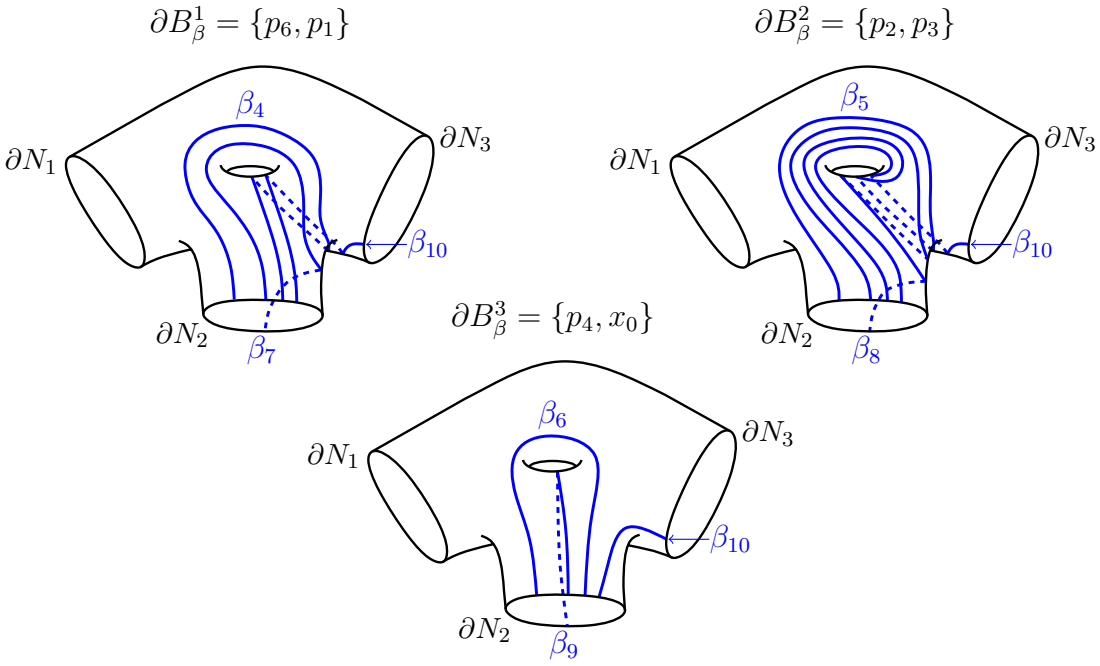

Figure 4.6: Pieces of $\boldsymbol{\beta}$ curves in $V \times \Sigma_{h,3}$

Similarly, for the $\boldsymbol{\gamma}$ curves, recall that for $1 \leq j \leq 2$ and $1 \leq i \leq 3$, the curve γ_{3j+i} contains the arcs $\{p_{2k_i-1}\} \times \tilde{\varphi}(\overline{t_\alpha^i})(\omega_\gamma^j)$ and $\{p_{2k_i}\} \times \tilde{\varphi}(\overline{t_\alpha^{i+1}})(\omega_\gamma^j)$, while the curve γ_{10} contains $\sqcup_{i=1}^{3-\chi}\left(\partial B_\alpha^i \times \tilde{\varphi}(\overline{t_\alpha^i})(\mathcal{C}_\gamma)\right)$. From (4.4) and the definition of $\tilde{\varphi}$, we have $\tilde{\varphi}(\overline{t_\alpha^1}) = (\tau_{\mu\ell})^{-1}$, $\tilde{\varphi}(\overline{t_\alpha^2}) = \tau_{\mu\ell}$, and $\tilde{\varphi}(\overline{t_\alpha^3}) = 1$. Unlike with the $\boldsymbol{\beta}$ curve system, the two endpoints of each B_γ^i have different images of $\boldsymbol{\gamma}$ arcs, all labeled in Figure 4.7.

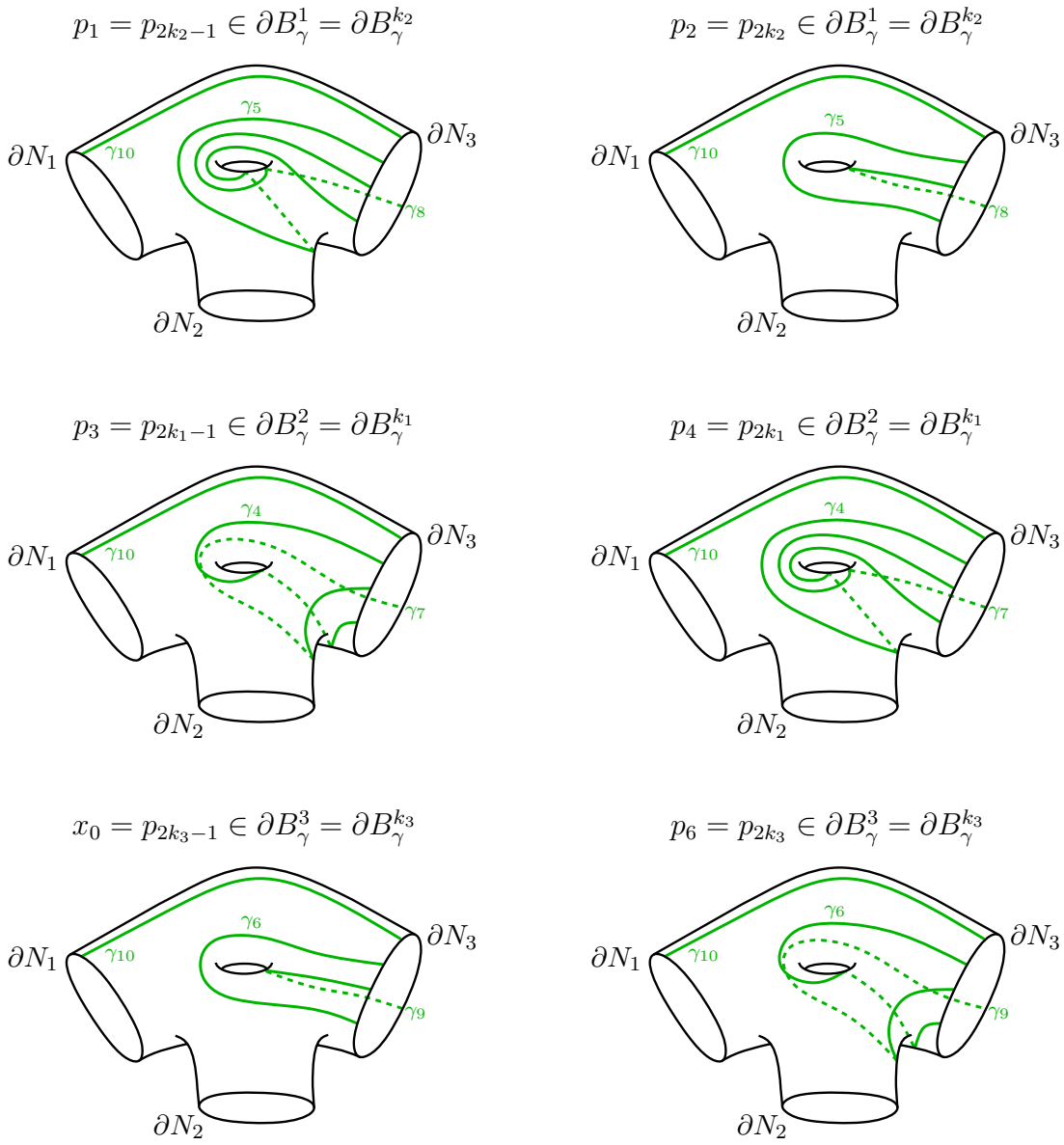

Figure 4.7: Pieces of $\boldsymbol{\gamma}$ curves in $V \times \Sigma_{h,3}$

We now proceed with the placement of curves in $\Sigma \cong \Sigma_{10}$. Figure 4.8 shows two copies of the trisection surface, one with pieces labeled corresponding to the description of Σ given in the proof of Lemma 4.5, and the other containing the curves from step 3 of the algorithm. Note that in the construction of Σ, the copies of the fiber are rotated or reflected to respect the orientations on the 1-skeleton of the base.

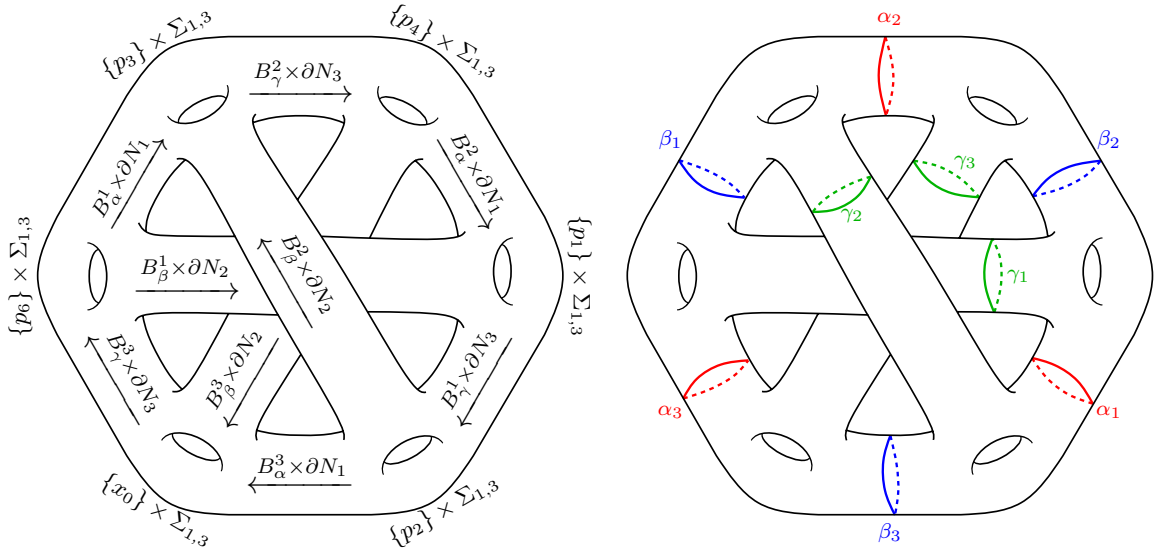

Figure 4.8: A trisection surface for $T^2 \times_{\tilde{\varphi}} T^2$, and the first curves from the algorithm

We build the remaining curves from the arcs that we constructed previously. In particular, the $\boldsymbol{\alpha}$ arcs in Figure 4.5 will be embedded in each component of $V \times \Sigma_{1,3}$, with the endpoints connected across $B_\alpha \times \partial N_1$ or $B_\beta \times \partial N_2$ (see Figure 4.9a). The $\boldsymbol{\beta}$ and $\boldsymbol{\gamma}$ arcs from Figures 4.6 and 4.7, respectively, will be embedded in the appropriate components of $V \times \Sigma_{1,3}$, and the endpoints will be connected across $B_\beta \times \partial N_2$, $B_\gamma \times \partial N_3$, or $B_\alpha \times \partial N_1$ as necessary. The remaining $\boldsymbol{\gamma}$ curves are shown in Figure 4.9b; Figure 4.10a shows the remaining $\boldsymbol{\beta}$ curves, while a curve system that is handle-slide equivalent to $\boldsymbol{\beta}$ is shown in Figure 4.10b. In each of these figures, note how the arc embeddings respect the reflections that have occurred among the components of $V \times \Sigma_{1,3}$.

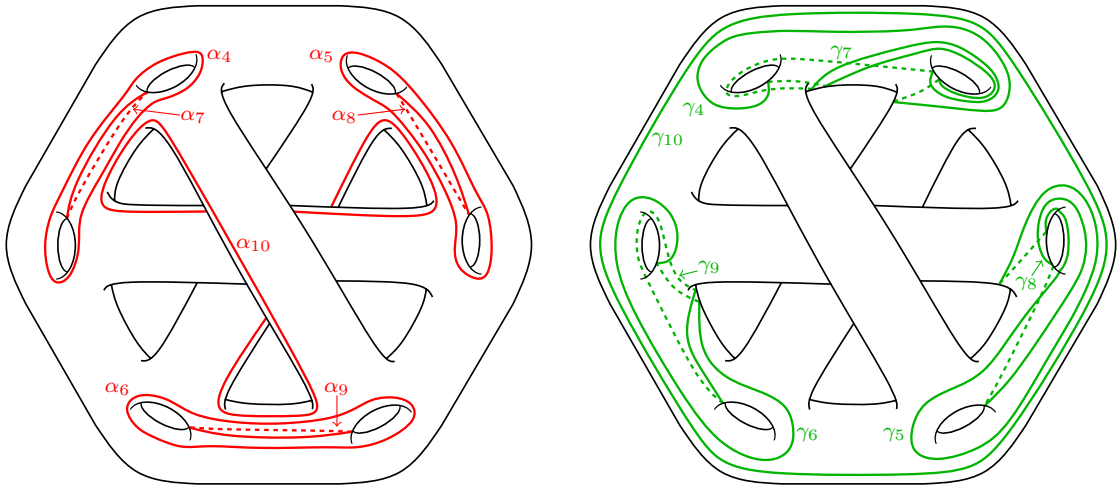

(a) $\boldsymbol{\alpha}$ curves for $T^2 \times_{\tilde{\varphi}} T^2$ (b) $\boldsymbol{\gamma}$ curves for $T^2 \times_{\tilde{\varphi}} T^2$

Figure 4.9: Two partial sets of curves for $T^2 \times_{\tilde{\varphi}} T^2$

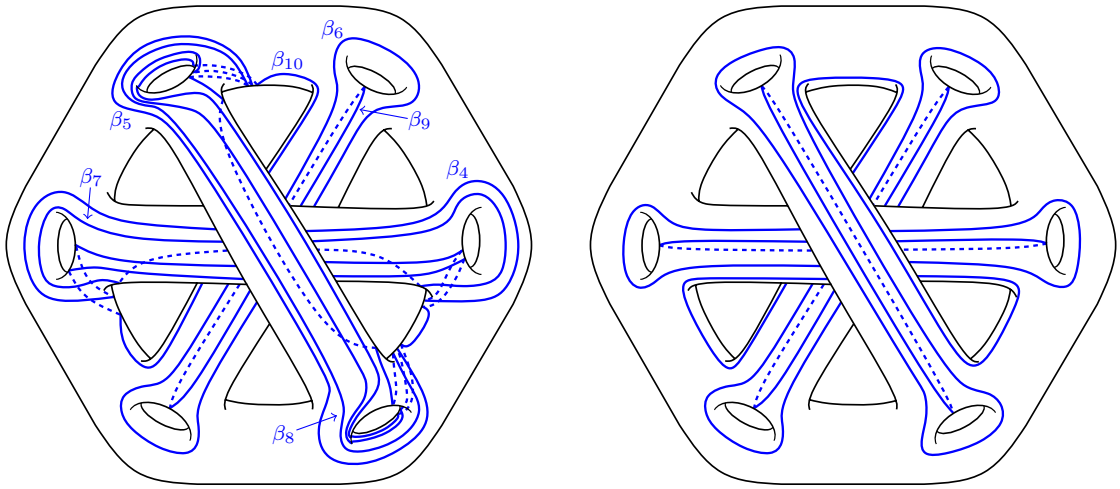

(a) $\boldsymbol{\beta}$ curves for $T^2 \times_{\tilde{\varphi}} T^2$ (b) A slide-equivalent curve system

Figure 4.10: A third partial set of curves for $T^2 \times_{\tilde{\varphi}} T^2$

Finally, we obtain the trisection diagram for $T^2 \times_{\tilde{\varphi}} T^2$ shown in Figure 4.11 from the curves in Figures 4.8, 4.9, and 4.10b.

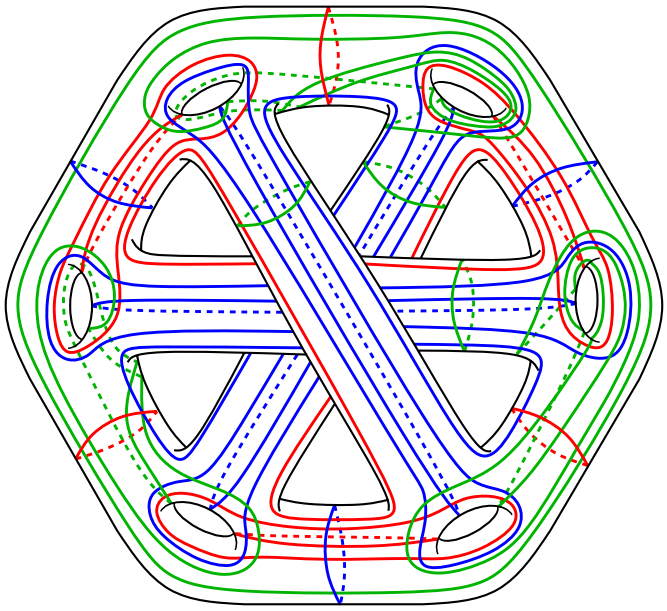

Figure 4.11: A trisection diagram for $T^2 \times_{\tilde{\varphi}} T^2$

4.3 Proof that diagram and trisection coincide

In this section, we use descriptions of the pairwise intersections $X_i \cap X_{i+1}$ and of the trisection surface Σ given in the proofs of Lemmas 4.4 and 4.5 to see that the curves defined in Section 4.2 define the same trisected 4-manifold as Theorem 4.3. Throughout this section, we consider the local product structure on Σ relative to the trivial bundle structure on $p^{-1}(B_2) = B_2 \times \Sigma_h$. For convenience, we consider each curve system separately.

4.3.1 $\boldsymbol{\alpha}$ curves

We first demonstrate that each curve in $\boldsymbol{\alpha} = (\alpha_1, \ldots, \alpha_{(3-\chi)(2h+1)+1})$ bounds a disk in $X_1 \cap X_2$. Consider $X_1 \cap X_2$ as the union of

$$X_1 \cap \overline{p^{-1}(B_2) \setminus \nu_2} = \left(B_\alpha \times \overline{\Sigma_h \setminus (N_1 \sqcup N_2)}\right) \cup (B_2 \times \partial N_2)\,,$$

a genus $(3-\chi)(2h)+1$ handlebody inside $p^{-1}(B_2) = B_2 \times \Sigma_h$, and

$$X_1 \cap \nu_3 \cong B_\gamma \times N_3,$$

$3-\chi$ 1-handles contained in $p^{-1}(B_\gamma)$. Each of these 1-handles has a co-core of the form $\{b_\gamma^i\} \times N_3$ with boundary α_i for some $1 \leq i \leq 3-\chi$; these $\boldsymbol{\alpha}$ curves are unaffected by the monodromy. Thus, the same arguments used in the proof of Lemma 3.13 work here to show that $\boldsymbol{\alpha}$ is a defining set of curves for $X_1 \cap X_2$.

4.3.2 $\boldsymbol{\beta}$ curves

We now turn to the $\boldsymbol{\beta}$ curves, which bound disks in $X_2 \cap X_3$. We consider $X_2 \cap X_3$ as the union of

$$\overline{p^{-1}(B_2) \setminus \nu_2} \cap X_3 = \left(B_\beta \times \overline{\Sigma_h \setminus (N_2 \sqcup N_3)}\right) \cup (B_\alpha \times N_1), \tag{4.5}$$

a genus $(3-\chi)(2h)+1$ handlebody inside $p^{-1}(B_2)$, and

$$\nu_3 \cap X_3 = \partial\nu_3 \cong B_3 \times \partial N_3, \tag{4.6}$$

a solid torus contained in $p^{-1}(B_3)$.

For $1 \leq i \leq 3-\chi$, the curve

$$\beta_i = \{b_\alpha^i\} \times \partial N_1$$

bounds the disk $\{b_\alpha^i\} \times N_1$, which is a co-core of the 1-handle $B_\alpha^i \times N_1$ inside $B_\alpha \times N_1$, a subset of $p^{-1}(B_2)$, as shown in (4.5). Additionally, for each $1 \leq j \leq 2h$ and each

$1 \leq i \leq 3-\chi$, the curve

$$\beta_{(3-\chi)j+i} = (\partial B^i_\beta \times \tilde{\varphi}(t^i_\beta)(\omega^j_\beta)) \cup (B^i_\beta \times \partial \omega^j_\beta)$$

bounds the product disk $B^i_\beta \times \tilde{\varphi}(t^i_\beta)(\omega^j_\beta)$ inside $B_\beta \times \overline{\Sigma_h \setminus (N_2 \sqcup N_3)}$, which is again contained in $p^{-1}(B_2)$.

The final $\boldsymbol{\beta}$ curve is

$$\beta_{(3-\chi)(2h+1)+1} = \sqcup_{i=1}^{3-\chi} \left(\partial B_\beta \times \tilde{\varphi}(t^i_\beta)(\mathcal{C}_\beta)\right) \cup (B_\beta \times \{c^1_\beta\}) \cup (B_\gamma \times \{c^2_\beta\}).$$

Consider the disk $(B_3 \times \{c^2_\beta\}) \cup (B_\beta \times \mathcal{C}_\beta)$, viewed as a subset of $p^{-1}(B_3) \cong B_3 \times \Sigma_h$. We claim that $\beta_{(3-\chi)(2h+1)+1}$ is the boundary of this disk, which is properly embedded in $X_2 \cap X_3$. First note that $B_3 \times \{c^2_\beta\}$ is a meridional disk of the solid torus $B_3 \times \partial N_3$ inside $B_3 \times \Sigma_h$, as described in (4.6). Now, for each $1 \leq i \leq 3-\chi$, we take the boundary arc $B^i_\beta \times \{c^2_\beta\}$ of this meridional disk and attach the disk $B^i_\beta \times \mathcal{C}_\beta$ inside $p^{-1}(B_3)$. We thus replace each arc $B^i_\beta \times \{c^2_\beta\}$ with the corresponding union of arcs $(\{p_{2i-2}\} \times \mathcal{C}_\beta) \cup (B^i_\beta \times \{c^1_\beta\}) \cup (\{p_{2i-1}\} \times \mathcal{C}_\beta)$ in $B_3 \times \Sigma_h$. Finally, we map these arcs back to $B_2 \times \Sigma_h$ to see how they lie in Σ. From the definition of X as a flat bundle, we see that $\partial B^i_\beta \times \mathcal{C}_\beta$ in $B_3 \times \Sigma_h$ is identified with $\partial B^i_\beta \times \tilde{\varphi}(t^i_\beta)(\mathcal{C}_\beta)$ in $B_2 \times \Sigma_h$. Since each $\tilde{\varphi}(t^i_\beta)$ fixes $\partial \mathcal{C}_\beta$ pointwise (by Remark 4.9), the boundary of this disk is exactly $\beta_{(3-\chi)(2h+1)+1}$. See Figure 4.12a.

Remark 4.12. This collection of $\boldsymbol{\beta}$ curves is handle-slide equivalent to the set of $\boldsymbol{\beta}$ curves from the algorithm for the trivial bundle, as it was in Example 4.11 with Figure 4.10. It follows that $\boldsymbol{\beta}$ is a defining set of curves for $X_2 \cap X_3$.

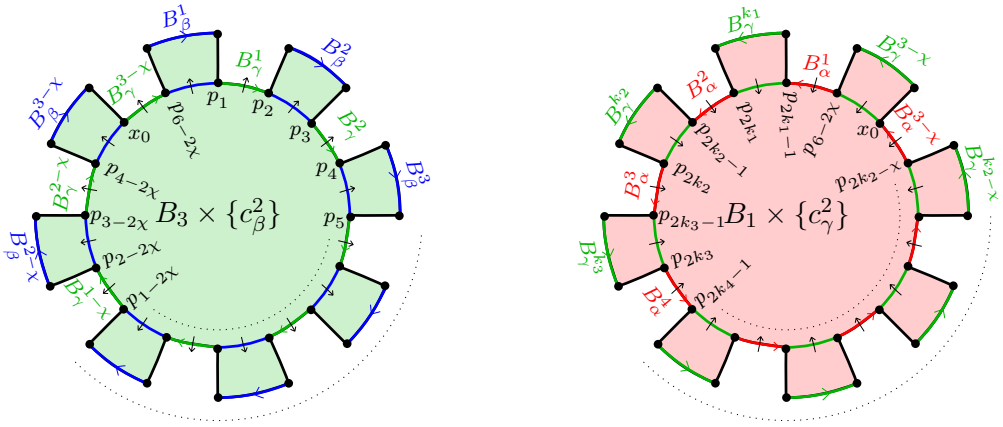

(a) (b)

Figure 4.12: At left: a schematic of the disk bounded by $\beta_{(3-\chi)(2h+1)+1}$ in $B_3 \times \Sigma_h$. B_β, B_γ, and $\mathcal{C}_\beta$ are depicted in blue, green, and black, respectively. At right: a schematic of the disk bounded by $\gamma_{(3-\chi)(2h+1)+1}$ in $B_1 \times \Sigma_h$. B_α, B_γ, and $\mathcal{C}_\gamma$ are depicted in red, green, and black, respectively. Edge orientations and transversality are indicated with arrows.

4.3.3 γ curves

With our consideration of $X_3 \cap X_1$, we will find it convenient to work largely in $p^{-1}(B_1)$ before translating to $p^{-1}(B_2)$, similar to how we used $p^{-1}(B_3)$ to see the disk in $X_2 \cap X_3$ bounded by $\beta_{(3-\chi)(2h+1)+1}$. In particular, we have $X_3 \cap X_1$ as the union of

$$X_3 \cap \overline{p^{-1}(B_1) \setminus \nu_1} \cong (B_\gamma \times \overline{\Sigma_h \setminus (N_3 \sqcup N_1)}) \cup (B_1 \times \partial N_1),$$

a genus $(3-\chi)(2h)+1$ handlebody inside $p^{-1}(B_1)$, and

$$X_3 \cap \nu_2 = B_\beta \times N_2,$$

a collection of $3-\chi$ 1-handles inside $p^{-1}(B_\beta) \subseteq p^{-1}(B_2)$. For each $1 \leq i \leq 3-\chi$, we have the curve $\gamma_i = \{b^i_\beta\} \times \partial N_2$ bounding the disk $\{b^i_\beta\} \times N_2$, which is a co-core of the 1-handle $B^i_\beta \times N_2$.

Now, given $1 \leq j \leq 2h$ and $1 \leq i \leq 3-\chi$, consider the disk $B_\gamma^{k_i} \times \omega_\gamma^j$ in $B_1 \times \Sigma_h \cong p^{-1}(B_1)$. Recall from Section 4.2 that the edge $B_\gamma^{k_i}$ starts at p_{2k_i-1}, the terminal vertex of edges B_α^i and $B_\beta^{k_i}$, and ends at p_{2k_i}, the initial vertex of edges B_α^{i+1} and $B_\beta^{k_i+1}$. It follows that the boundary arc

$$\{p_{2k_i-1}\} \times \omega_\gamma^j$$

as an arc in $\partial B_\alpha^i \times \Sigma_h \subset B_1 \times \Sigma_h$ is identified with

$$\{p_{2k_i-1}\} \times \tilde{\varphi}(\overline{t_\alpha^i})(\omega_\gamma^j)$$

as an arc in $\partial B_\beta^{k_i} \times \Sigma_h \subset B_2 \times \Sigma_h$. Likewise, the arc $\{p_{2k_i}\} \times \omega_\gamma^j$ in $\partial B_\alpha^{i+1} \times \Sigma_h \subset B_1 \times \Sigma_h$ is identified with the arc $\{p_{2k_i}\} \times \tilde{\varphi}(\overline{t_\alpha^{i+1}})(\omega_\alpha^j)$ in $\partial B_\beta^{k_i+1} \times \Sigma_h \subset B_2 \times \Sigma_h$. Hence, for each $1 \leq j \leq 2h$ and each $1 \leq i \leq 3-\chi$, the curve

$$\gamma_{(3-\chi)j+i} = \left(\{p_{2k_i-1}\} \times \tilde{\varphi}(\overline{t_\alpha^i})(\omega_\gamma^j)\right) \cup \left(B_\gamma^{k_i} \times \partial\omega_\gamma^j\right) \cup \left(\{p_{2k_i}\} \times \tilde{\varphi}(\overline{t_\alpha^{i+1}})(\omega_\gamma^j)\right)$$

bounds the disk $B_\gamma^{k_i} \times \omega_\gamma^j$ inside $B_1 \times \Sigma_h$.

Our final $\boldsymbol{\gamma}$ curve,

$$\gamma_{(3-\chi)(2h+1)+1} = \sqcup_{i=1}^{3-\chi} \left(\partial B_\alpha^i \times \tilde{\varphi}(\overline{t_\alpha^i})(\mathcal{C}_\gamma)\right) \cup (B_\gamma \times \{c_\gamma^1\}) \cup (B_\alpha \times \{c_\gamma^2\}),$$

forms the boundary of $(B_1 \times \{c_\gamma^2\}) \cup (B_\gamma \times \mathcal{C}_\gamma)$, which is again a disk in $B_1 \times \Sigma_h$. See Figure 4.12b.

Once again, the arguments used in the proof of Lemma 3.13 apply to show that $\boldsymbol{\gamma}$ is a defining set of curves for $X_3 \cap X_1$.

CHAPTER 5

EXTENSIONS

In this chapter, we present some open questions in an attempt to relate the constructions in Chapters 3 and 4 to existing work in other areas of trisection theory. In Section 5.1, we consider the potential relationship between different bundle structures on a given 4-manifold X, specifically when X fibers as a surface bundle over T^2 and as a 3-manifold bundle over S^1. Section 5.2 addresses the possibility of strengthening Proposition 4.6 and further classifying the trisection genus of nontrivial flat surface bundles over surfaces. We end the chapter with a closer look at relative trisections of compact manifolds in Section 5.3, and a question of whether the methods of Chapter 4 can be extended to manifolds with boundary.

5.1 Connections to 3-manifold bundles over S^1

Koenig has shown that a 3-manifold bundle over S^1 admits a $(3g+1; g+1)$-trisection whenever the bundle monodromy preserves or flips a genus g Heegaard splitting of the 3-manifold M [Koe17]. In the case where M is a Σ_h-bundle over S^1, classical Heegaard theory tells us that M admits a genus $(2h+1)$ Heegaard splitting, and that this splitting is minimal when the rank of $\pi_1(M)$ is $2h+1$, as with trivial bundles or closed bundles where the monodromy is a sufficiently large power of a pseudo-Anosov

map (see [Sch93, Rub05]).

Taking a closer look at 4-dimensional trivial bundles within this framework, we consider 4-manifolds of the form $T^2 \times \Sigma_h = X = S^1 \times (S^1 \times \Sigma_h)$. Applying Theorem 3.3 to the first perspective here, we have a fiber surface of genus h and a base surface of genus $g = 1$, giving us a $(3(2h+1)+1; 2+2h)$-trisection of $T^2 \times \Sigma_h$. For the latter perspective, we know the standard Heegaard splitting of $S^1 \times \Sigma_h$ is minimal and has genus $2h+1$; this splitting is preserved by the (trivial) bundle monodromy in this case, and hence, we get a $(3(2h+1)+1; 2h+2)$-trisection of $S^1 \times (S^1 \times \Sigma_h)$ by Koenig [Koe17]. The parameter values agree in these two cases, and both trisections are minimal by Theorem 3.17. However, it is not obvious whether the trisection diagrams arising from the two different algorithms are related solely by handle slides and diffeomorphism, without the need for stabilization or destabilization. Hence, we ask:

Question 5.1. Does $X = T^2 \times \Sigma_h$ have a unique minimal trisection $\mathcal{T}$, in the sense that every trisection of X is handle slide and diffeomorphism equivalent to a stabilization of $\mathcal{T}$? In particular, does trisecting X as a 3-manifold bundle over S^1 following Koenig's construction [Koe17] give the same trisection as Theorem 3.3?

More generally, we consider 4-manifolds X which fiber nontrivially as $\Sigma_h \to X \to T^2$ and as $M \to X \to S^1$, with $\Sigma_h \to M \to S^1$. Since there are 3-manifolds $\Sigma_h \to M \to S^1$ with Heegaard genus two for arbitrarily large h [HT85], we expect there to be 3-manifolds $\Sigma_h \to M \to S^1$ and 4-manifolds $M \to X \to S^1$ for which a genus $g \neq 2h+1$ splitting of M is minimal with respect to the bundle monodromy of X preserving or flipping the splitting, as required by Koenig's construction. Such a pair (M, X) would yield a trisection of $\Sigma_h \to X \to T^2$ with different parameters than those obtained in Theorem 4.3.

Question 5.2. Suppose X fibers as a Σ_h-bundle over T^2 and as a M-bundle over S^1, where M is itself a Σ_h-bundle over S^1. Suppose further that this second fibration of X has a bundle monodromy that flips or preserves a genus g Heegaard splitting of M, and that g is minimal with respect to this property. Let $\mathcal{T}$ denote the $(3(2h+1)+1; 2+2h)$-trisection of X given by Theorem 4.3, and let $\mathcal{T}'$ denote the $(3g+1; g+1)$-trisection of X given in [Koe17].

1. If $g < 2h+1$, then $\mathcal{T}$ is not minimal. In this case, is $\mathcal{T}$ stabilized? In particular, is $\mathcal{T}$ a stabilization of $\mathcal{T}'$?

2. If $g > 2h+1$, is $\mathcal{T}'$ a stabilization of $\mathcal{T}$?

3. If $g \geq 2h+1$, is $\mathcal{T}$ stabilized? How are $\mathcal{T}$ and $\mathcal{T}'$ related in this case?

Section 5.2 presents additional questions related to minimality, Question 5.2, and Proposition 4.6.

5.2 More on minimality

Theorem 3.17 asserts that for any choice of $g, h \geq 0$, the $((2g+1)(2h+1)+1; 2g+2h)$-trisection of $\Sigma_g \times \Sigma_h$ produced in Chapter 3 is minimal; the proof relies on the fact that the rank of $\pi_1(\Sigma_g \times \Sigma_h)$ is $2g+2h$. Chapter 4 produces a $((2g+1)(2h+1)+1; 2g+2h)$-trisection of any flat Σ_h-bundle over Σ_g, but the analogous minimality result is weaker: Proposition 4.6 states only that a sufficient condition for the trisection to be minimal is that the fundamental group of the bundle has rank $2g+2h$. It is not obvious if that condition is necessary or when it holds:

Question 5.3. Theorem 4.3 puts an upper bound of $(2g+1)(2h+1)+1$ on the trisection genus of a flat Σ_h-bundle over Σ_g. When is that bound sharp? In general, what is the trisection genus of a given nontrivial flat Σ_h-bundle over Σ_g?

A related question follows once a bundle with a lower trisection genus has been identified (potential candidates are discussed in Section 5.1). While any two trisections of that bundle are stably isotopic by Theorem 1.1, there is no guarantee that a non-minimal trisection can be strictly destabilized down to a minimal trisection. It is feasible that some combination of both destabilizations and stabilizations would need to be employed to obtain a trisection with minimal genus:

Question 5.4. For what bundles can the trisection defined in Theorem 4.3 be destabilized?

5.3 Relative trisections

Let X be a compact connected 4-manifold with connected boundary $\partial X \neq \emptyset$. A *relative trisection* of X is similar to a trisection of a closed manifold, but with slightly altered characteristics including a restriction on how each sector X_i intersects ∂X. The result is that the relative trisection structure induces an open-book decomposition on ∂X [GK16]. Relative trisection diagrams are also similar to the closed case, except that the surface now has boundary and the diagram may contain properly embedded arcs in addition to curves, although these arcs are not strictly necessary to reconstruct the original 4-manifold [CGPC18].

The constructions from Chapter 4 translate nicely to relative trisections of disk bundles over S^2, along with accompanying relative trisection diagrams [CGPC18, Example 5.1]. However, for a disk bundle over Σ_g with $g > 0$, the extra boundary conditions for a relative trisection cannot be met by the construction used in Theorem 4.3. In particular, a relative trisection has four non-negative parameters $(h, k; p, b)$,

satisfying the relations

$$2p + b - 1 \leq k \leq h + p + b - 1 \tag{5.1}$$

[CGPC18]; the trisection surface is $\Sigma_{h,b}$, the 4-dimensional sectors X_i are each diffeomorphic to $\natural^k(S^1 \times B^3)$, and the open-book decomposition on ∂X induced by the trisection has pages $\Sigma_{p,b}$. For a disk bundle over Σ_g, a decomposition of Σ_g as described in Lemma 3.1 gives $h = 2g + 2$, $k = 2g + 1$, and $b = 4g + 2$. Substituting these values into (5.1) yields the simplified relations

$$2p + 2g \leq 0 \leq 4g + 2 + p. \tag{5.2}$$

With non-negative parameters, the relations (5.2) are satisfied only when $p = g = 0$, thus precluding the possibility of the base surface having higher genus. To our knowledge, other variants of surface bundles over surfaces with base and fiber both compact have not yet been considered through the lens of trisection theory. We thus have a natural question on how the results in Chapter 4 might extend:

Question 5.5. Is there an adaptation of Theorem 4.3 to relative trisections of compact surface bundles over surfaces, in cases other than disk bundles over S^2?

APPENDIX A

EXAMPLES (DIAGRAMS)

A.1 Trivial bundles

The figures that follow are trisection diagrams for trivial bundles, obtained from the algorithm in Chapter 3 unless otherwise indicated.

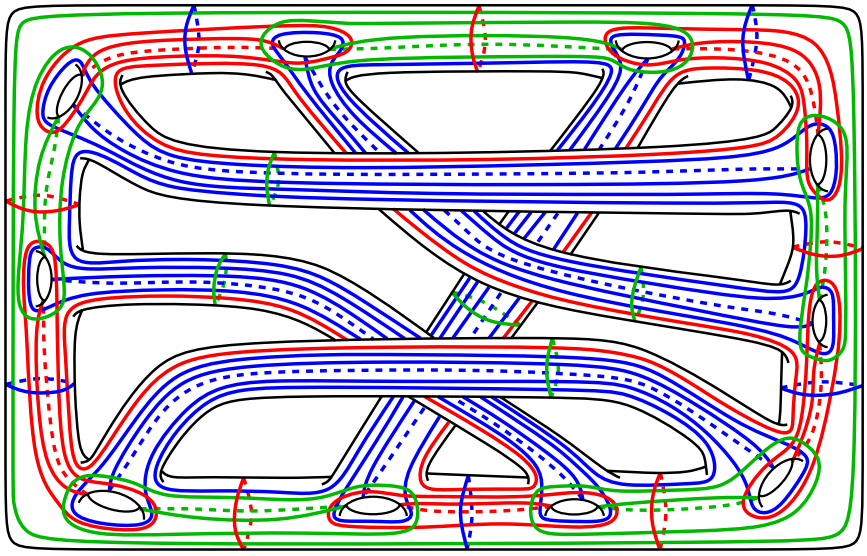

Figure A.1: A trisection diagram for $\Sigma_2 \times T^2$, viewed as the trivial T^2-bundle over Σ_2

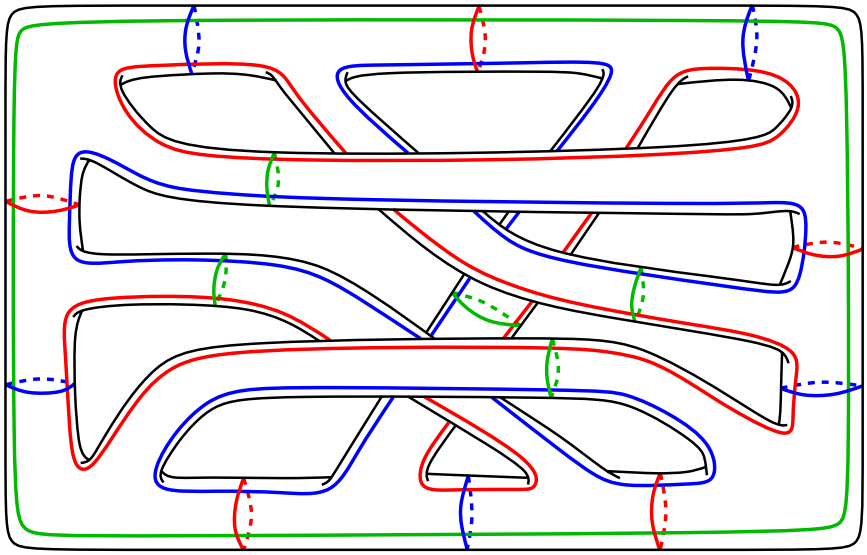

Figure A.2: A trisection diagram for $\Sigma_2 \times S^2$, viewed as the trivial S^2 bundle over Σ_2

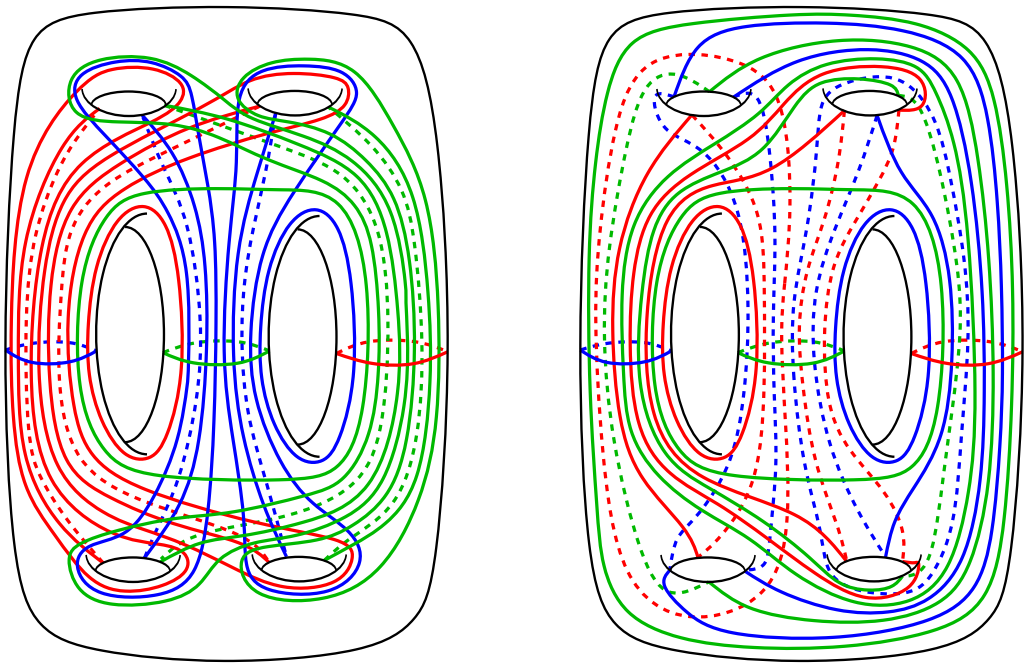

(a) (b)

Figure A.3: Two trisection diagrams for $S^2 \times \Sigma_2$, viewed as the trivial Σ^2-bundle over S^2. The first comes from the algorithm described in Chapter 3. The second is obtained from the first by a sequence of handle slides; this diagram is diffeomorphic to that given in Figure A.2

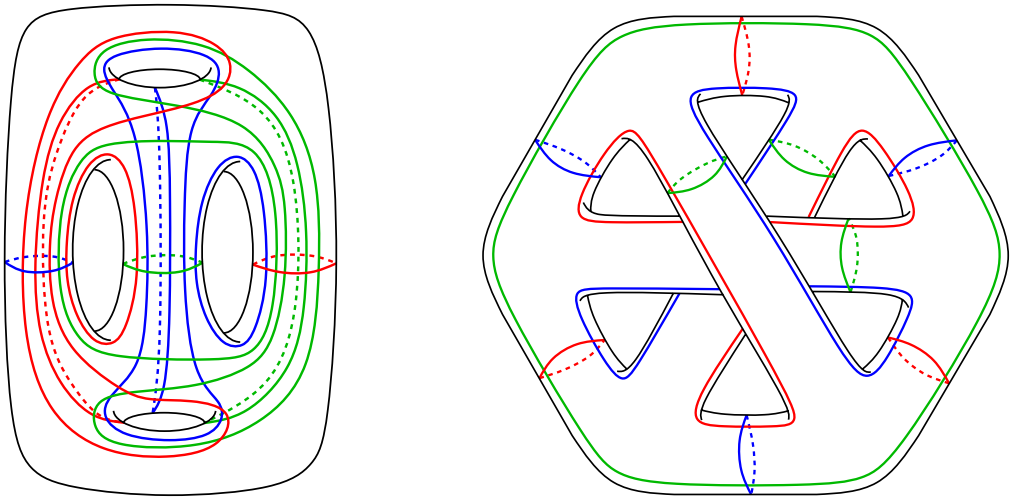

(a) (b)

Figure A.4: Two trisection diagrams for $S^2 \times T^2$, first viewed as the trivial T^2-bundle over S^2, and then as the trivial S^2-bundle over T^2

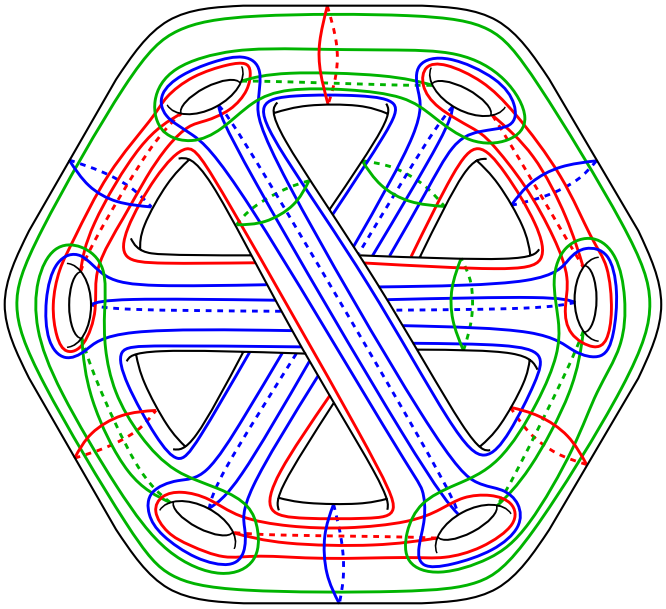

Figure A.5: A trisection diagram for $T^2 \times T^2$

A.2 Nontrivial bundles

The figures in this section are trisection diagrams for nontrivial bundles, obtained using the modified algorithm from Chapter 4, or the conjectured extension to bundles with non-orientable base.

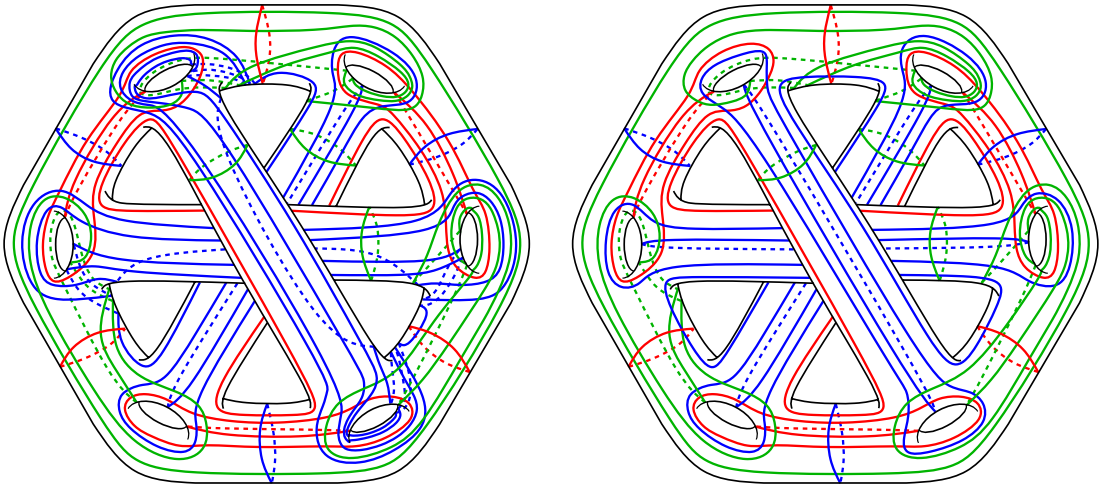

Figure A.6: A trisection diagram for $T^2 \times_{\tilde{\varphi}} T^2$, with $\tilde{\varphi}$ defined in Example 4.11. The diagram on the left is straight from the algorithm; the diagram on the right is handle-slide equivalent and appeared previously in Figure 4.11

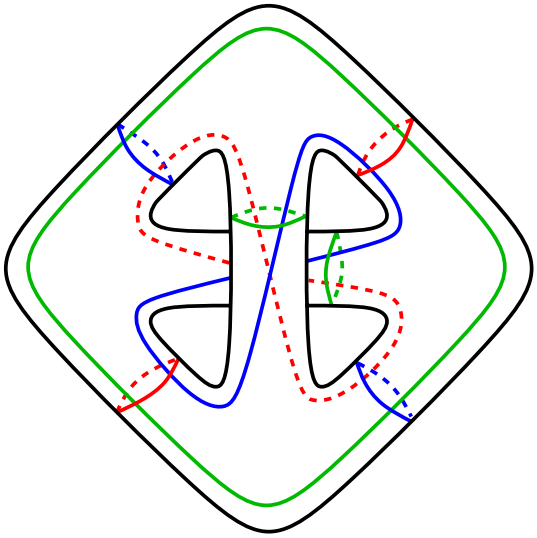

Figure A.7: A trisection diagram for $\mathbb{RP}^2 \tilde{\times} S^2$

Bibliography

[BR07] Mark Brittenham and Yo'av Rieck, *The heegaard genus of bundles over S^1*, Geom. Topol. Monogr. **12** (2007), 17–33.

[Cer70] J. Cerf, *La stratification naturelle des espaces de fonctions différentiables réelles et le théorème de la pseudo-isotopie*, Publ. Math. Inst. Hautes Études Sci. **39** (1970), 7–170.

[CGPC18] Nickolas A. Castro, David T. Gay, and Juanita Pinzón-Caicedo, *Diagrams for relative trisections*, Pacific J. Math. **294** (2018), no. 2, 275–305.

[CIMT19] Nickolas A. Castro, Gabriel Islambouli, Maggie Miller, and Maggy Tomova, *The relative $\mathcal{L}$-invariant of a compact 4-manifold*, arXiv:1908.05371v1, 2019.

[EE67] C. J. Earle and J. Eells, *The diffeomorphism group of a compact riemann surface*, Bull. Amer. Math. Soc. **73** (1967), no. 4, 557–559.

[FM12] Benson Farb and Dan Margalit, *A primer on mapping class groups*, Princeton Mathematical Series, vol. 49, Princeton University Press, 2012.

[GK16] David Gay and Robion Kirby, *Trisecting 4-manifolds*, Geom. Topol. **20** (2016), no. 6, 3097–3132.

[Gom83] Robert E. Gompf, *Three exotic $\mathbb{R}^4$'s and other anomalies*, J. Differential Geom. **18** (1983), no. 2, 317–328.

[GS99] Robert E. Gompf and András I. Stipsicz, *4-manifolds and kirby calculus*, Graduate Studies in Mathematics, vol. 20, American Mathematical Society, 1999.

[Hat02] Allen Hatcher, *Algebraic topology*, Cambridge University Press, 2002.

[HT85] A. Hatcher and W. Thurston, *Incompressible surfaces in 2-bridge knot complements*, Invent. Math. **79** (1985), 225–246.

[Koe17] Dale Koenig, *Trisections of 3-manifold bundles over S^1*, arXiv:1710.04345v1, 2017.

[LP72] François Laudenbach and Valentin Poénaru, *A note on 4-dimensional handlebodies*, Bull. Soc. Math. France **100** (1972), 337–344.

[Mei18] Jeffrey Meier, *Trisections and spun 4-manifolds*, Math. Res. Lett. **25** (2018), no. 5, 1497–1524.

[Mil11] John Milnor, *Differential topology 46 years later*, Notices Amer. Math. Soc. **58** (2011), no. 6, 804–809.

[MSZ16] Jeffrey Meier, Trent Schirmer, and Alexander Zupan, *Classification of trisections and the Generalized Property R Conjecture*, Proc. Amer. Math. Soc. **144** (2016), no. 11, 4983–4997.

[MT19] Kathryn Mann and Bena Tshishiku, *Realization problems for diffeomorphism groups*, Proc. Sympos. Pure Math. **102** (2019), 131–156.

[MZ17] Jeffrey Meier and Alexander Zupan, *Genus-two trisections are standard*, Geom. Topol. **21** (2017), no. 3, 1583–1630.

[Rei33] Kurt Reidemeister, *Zur dreidimensionalen Topologie. (German)*, Abh. Math. Semin. Univ. Hambg. **9** (1933), no. 1, 189–194.

[Rub05] J. Hyam Rubinstein, *Minimal surfaces in geometric 3-manifolds*, Global theory of minimal surfaces: Clay Math. Proc. **2** (2005), 725–746.

[Sch93] Jennifer Schultens, *The classification of Heegaard splittings for (compact orientable surface)* $\times S^1$, Proc. London Math. Soc. **67** (1993), no. 3, 425–448.

[Sch01] Martin Scharlemann, *Heegaard splittings of compact 3-manifolds*, Handbook of Geometric Topology (R.J. Daverman and R.B. Sher, eds.), Elsevier, 2001, pp. 921–953.

[Sin33] James Singer, *Three-dimensional manifolds and their Heegaard diagrams*, Trans. Amer. Math. Soc. **35** (1933), no. 1, 88–111.

[ST93] Martin Scharlemann and Abigail Thompson, *Heegaard splittings of (surface)* $\times I$ *are standard*, Math. Ann. **295** (1993), no. 3, 549–564.

[ST20] Nick Salter and Bena Tshishiku, *Surface bundles in topology, algebraic geometry, and group theory*, Notices Amer. Math. Soc. **67** (2020), no. 2, 146–154.